■連載—脳神経外科医療の translational research (6)

脳・神経刺激療法の translational research

深谷　親　　片山　容一

NEUROLOGICAL SURGERY
脳神経外科
(文献略称：No Shinkei Geka)

第35巻　第4号　別刷
2007年4月10日　発行

医学書院

Neuromodulation

Technology at the Neural Interface

VOLUME XI • NUMBER 2 • APRIL 2008

Samuel J. Hassenbusch III, MD, PhD
1954-2008
In Memoriam

Journal of the International Neuromodulation Society

Official Journal of the International Functional Electrical Stimulation Society

Volume 11 • Number 2 • 2008
http://www.blackwell-synergy.com/loi/ner

ORIGINAL ARTICLE

Effect of Subthalamic Nucleus Stimulation on Severe Striatal Hand Deformity in Parkinson's Disease: A Case Report

Takashi Morishita, MD[1,2] • Yoichi Katayama, MD, PhD[1,2] • Kazutaka Kobayashi, MD, PhD[1,2] • Hideki Oshima, MD, PhD[1] • Chikashi Fukaya, MD, PhD[1,2] • Takamitsu Yamamoto, MD, PhD[1,2]

[1]*Division of Neurosurgery, Department of Neurological Surgery, and* [2]*Division of Applied System Neuroscience, Department of Advanced Medical Science, Nihon University School of Medicine, Tokyo, Japan*

ABSTRACT

Striatal hand is a deformity encountered in Parkinson's disease and other parkinsonisms. It is characterized by extension that occurs at all the interphalangeal joints, flexion at the metacarpophalangeal joints, and ulnar deviation. It can be differentiated from levodopa-induced dystonia and primary dystonia, since the deformity exists continuously even during sleep. We experienced a case of Parkinson's disease with severe striatal hand deformity which was successfully treated by deep brain stimulation of the subthalamic nucleus (STN-DBS). Although the precise mechanism remains unclear, rigidity is assumed to contribute to the limb deformities. Based on our experience, it seems possible therefore that the effect of STN-DBS on the hand deformity was a secondary effect on muscular rigidity. STN-DBS is assumed to represent a useful treatment option for striatal hand deformity.

KEY WORDS: *Deep brain stimulation, dystonia, Parkinson's disease, striatal deformity, subthalamic nucleus.*

Introduction

Charcot (1877) first reported the deformities of the hands and feet that are unique to Parkinson's disease (PD) (1). The hand deformities are typically characterized by extension that occurs at all the interphalangeal joints, flexion at the metacarpophalangeal joints, and ulnar deviation. The feet are described as showing claw-like deformities that accompany extension of the first and flexion of the second phalanges. They resemble rheumatoid arthritis, but do not display osteogenic changes and are negative for rheumatoid factor. Similar deformities can also be seen in other parkinsonisms which involve neostriatal pathophysiological abnormalities such as multiple system atrophy, progressive supranuclear palsy, and corticobasal degeneration, and they are thus called striatal hand or foot. Ashour et al. suggested that the terms striatal hand and foot be used to describe the features of these distal limb deformities in parkinsonism (2). Striatal limb deformity can be the first sign of PD, and is therefore differentiated from dopa-induced dystonia. Primary dystonia is often induced by action. On the other hand, striatal deformities exist continuously even during sleep. However, it remains still controversial as to whether the deformity constitutes primary dystonia or not (2,3).

Submitted: April 8 2007, 2006; accepted: July 31, 2007. Address correspondence and reprint requests to: Takamitsu Yamamoto, MD, PhD, Department of Neurological Surgery, Nihon University School of Medicine, 30-1 Oyaguchi Kamimachi, Itabashi-ku, Tokyo 173-8610, JAPAN. Email: nusmyama@med.nihon-u.ac.jp

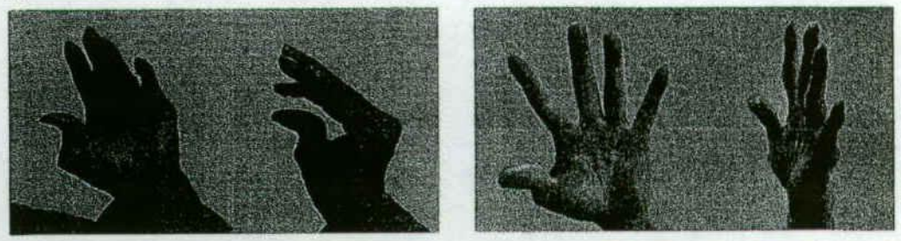

FIGURE 1. Left hand posture before deep brain stimulation of the subthalamic nucleus (STN-DBS) (A) and three years after STN-DBS (B). The patient could not extend the interdigital spaces before STN-DBS. However, after STN-DBS, he could open his palm easily and extend the interdigital spaces.

These deformities are clinically important in terms of the patient's activities of daily living and quality of life. There have been reports concerning various treatment options, such as botulinum toxin (4), orthopedic surgical interventions (5), and stereotactic thalamotomy (6). Deep brain stimulation (DBS) is now regarded as one of the effective treatment options for PD, and an effect on bradykinesia, rigidity, tremor, and dyskinesia has been demonstrated. To the best of our knowledge, there have been few reports focusing on the effect of DBS of the subthalamic nucleus (STN) on striatal hand deformity. Among our over 300 cases of STN-DBS, we have experienced several cases of PD with striatal limb deformities. We describe here a case of PD with one of the severest hand deformities which was treated by chronic STN-DBS.

Case Report

The patient was a 79-year-old man who had remained in his usual state of health until 1997, when he noticed deformity of his left hand first, and tremor occurred later on. He was diagnosed as having PD, and antiparkinsonian drugs were initiated in 1998. His symptoms progressed gradually to include motor fluctuations and wearing-off periods. He was intolerant to levodopa because of gastrointestinal side-effects, so he was able to receive a small dose of antiparkinsonian drugs. Finally, he was referred to our hospital and admitted for an operation in March 2004.

On admission, the patient's Hoehn and Yahr stage and the Unified Parkinson's Disease Rating Scale (UPDRS) were evaluated with optimal medications (7). His Hoehn and Yahr stage during the on period was III and that during the off period was IV. His total UPDRS scores during the on and off periods were 35 and 48, respectively. Based on these results, he was adjudged to be a good candidate for STN-DBS.

On examination, he displayed severe resting tremor and rigidity that were dominant on the left side. He also had deformity of his left hand (Fig. 1A) and was unable to hold anything with his left hand. The interphalangeal joints were extended and the metacarpophalangeal joints were flexed. The range of motion was restricted in the metacarpophalangeal joints of the left hand. Ulnar deviations were remarkable in the fifth finger of the left hand, and the deformity of the thumb exhibited fixed contracture. A hand X-ray showed none of the osteogenic changes that should be seen in rheumatoid arthritis, but dislocation of the distal interphalangeal joint of the thumb was observed (Fig. 2A). The deformity existed at rest even during sleep. Nerve conduction studies revealed that the peripheral nerves were intact. The deformity could be distinguished from dopa-induced dystonia because of the observed history in which the deformity represented the first sign of PD, was fixed and did not respond to levodopa. Based on these findings, the hand deformity was diagnosed as striatal hand. The hand deformity was given a score of 4 on the scale of 0–4 according to the striatal hand rating scale (8).

Following bilateral STN-DBS, the tremor, rigidity, and motor fluctuations were alleviated and the wearing-off periods disappeared. The Hoehn and Yahr stage improved to I even during the off periods, and the total UPDRS scores were also dramatically improved: 16 during the on period and 18 during the off period, at one year after the surgery. The rigidity underwent improvement as shown in Table 1. In addition, the levodopa equivalent dose was reduced from 330 mg to 210 mg. The deformity could be distinguished from dopa-induced dystonia because of the observed history. The deformity represented the first sign of PD. In addition, the deformity was fixed and did not respond to levodopa. The joints of the left hand, especially the metacarpophalangeal joints, became straightened; and the range of motion of the left hand was increased. The striatal hand rating scale improved to 1. The patient is now able to pick up small objects with his left hand.

Discussion

Ashour et al. reported that 12.8% of patients with PD encountered striatal deformities (8), and the deformities

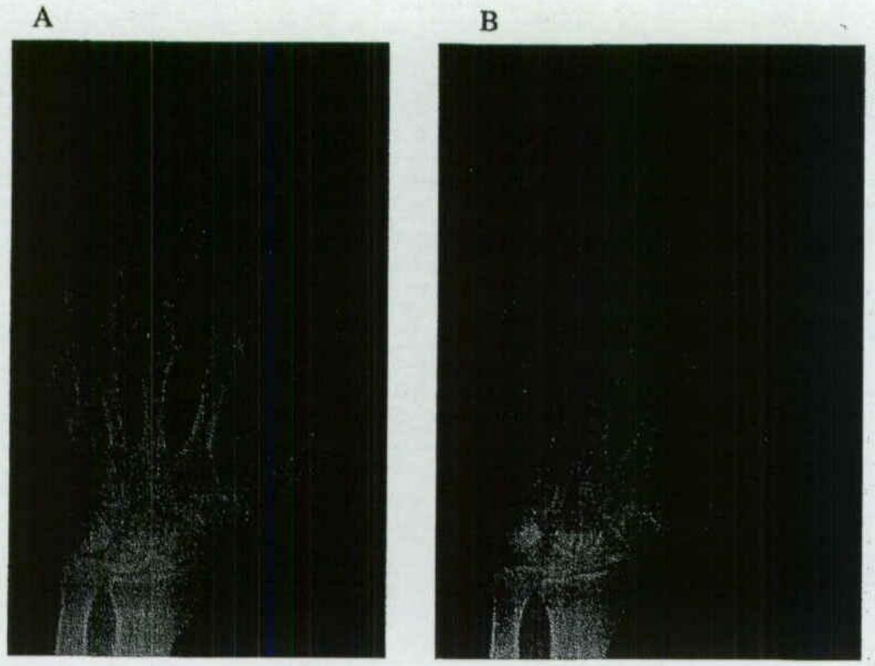

FIGURE 2. Left hand X-ray examinations before deep brain stimulation of the subthalamic nucleus (STN-DBS) (A) and three years after STN-DBS (B). Although the dislocated distal interphalangeal joint of the thumb did not show improvement due to fixed contracture, the interdigital spaces were clearly expanded after STN-DBS.

TABLE 1. Clinical Evaluations Before and After Deep Brain Stimulation of the Subthalamic Nucleus (STN-DBS)

	Before		One year after	
	On period	Off period	On period	Off period
Hoehn and Yahr stage	III	IV	II	II
Total UPDRS	35	48	16	18
UPDRS Part III	22	31	12	12
Item 22 (Rigidity)	10	10	0	0
Striatal hand rating scale	4		1	
Levodopa equivalent dose	330 mg		210 mg	

The Hoehn and Yahr stage, the Unified Parkinson's Disease Rating Scale (UPDRS), striatal hand rating scale, and levodopa equivalent dose were evaluated before and at one year after STN-DBS. A remarkable improvement was seen in the motor scores.

can be presented at the early stages of PD (1,8). Rigidity caused by lesions in the neostriatum has been considered to contribute to the etiology of the deformities as mentioned by Gowers (9), and another report has supported the existence of a correlation between rigidity and the deformities (10). Although the mechanism of the effect of STN-DBS on such deformity is unclear, improvement of the rigidity may contribute to the improvement of the deformity since we experienced dramatic improvement of rigidity as well as improvement of the hand deformity.

It is well known that certain dystonic postures besides striatal limb deformities and dopa-induced dystonic dyskinesia occur in PD (3). Striatal deformities are atypical for dystonia and classified as one of the atypical dystonias in PD (3). Striatal deformities exist continuously even during sleep. In contrast, primary dystonia does not present during sleep but is usually induced or exacerbated by a particular action or posture (2). In addition, striatal deformity usually accompanies other parkinsonian signs and symptoms. A long history of dystonia can also lead to fixed contracture, and, in this respect, it is difficult to distinguish striatal deformities from dystonia. As Chou described in a case of cervical dystonia successfully treated by STN-DBS (11), it is possible that STN-DBS is effective on dystonic pathophysiology. Therefore, it is possible that STN-DBS can be also effective for a dystonic etiology in our case.

Poewe et al. hypothesized that striatal somatotopic organization relates to rostrocaudal gradient of decreased dopamine and increased γ-aminobutyric acid in PD patient with dopa-induced dyskinesia (12) based on clinical experience and animal studies (13,14). Similarly, the relationship between rostrocaudal gradient of dopamine and somatotopy in the striatum might correlate with the fact that the deformities tend to occur in the distal part of the limb. A recent functional magnetic resonance imaging study also described the somatotopy in the human striatum (15). In addition, a positron emission tomography study showed increase in regional cerebral blood flow in the prefrontal cortex, putamen, and thalamus in PD patients after STN-DBS (16). Such effect on blood flow may also contribute to the improvement of the deformities.

Some other mechanisms such as an effect by ergot dopamine agonist and female hormone have been proposed. In our case, the hand deformity existed continuously even during sleep. In addition, our patient did not take ergot dopamine agonist and was a male.

The timing of initiating surgery for PD patients with limb deformities seems to be important. Hu et al. reported a PD patient with right upper limb contracture that was refractory to unilateral ventromedial pallidotomy (17). They described the patient as showing "moderate improvement in dyskinesias and 'off' period symptoms, but no change in the hand-arm contractures." They inferred that the timing of the pallidotomy was too late to improve the deformities. In this context, it may well be true that we initiated the STN-DBS in our case before the joint had reached contracture.

Improvement of motor function correlates with the quality of life of patients with PD. At the same time, improvement in the deformities is thought to contribute to improving the quality of life of such patients. STN-DBS is usually indicated for patients with advanced PD such as cases with severe side-effects of levodopa therapy. On the other hand, the deformities can be encountered even at the early stage of PD as we experienced, and they make the patient's quality of life worse. STN-DBS may thus be indicated in PD patients with limb deformities even at the early stage of their disease if it is resistant to any medications. Nevertheless, further research is needed to evaluate the exact effects and the enrollment of DBS for such deformities.

References

1. Charcot JM. *Lectures on the Diseases of the Nervous System, Lecture V.* London: New Sydenham Society, 1877.

2. Ashour R, Tintner R, Jankovic J. Striatal deformities of the hand and foot in Parkinson's disease. *Lancet Neurol* 2005;4:423–431.

3. Tolosa E, Compta Y. Dystonia in Parkinson's disease. *J Neurol* 2006;253:7003–7006.

4. Cordivari C, Misra VP, Cattania S, Lees AJ. Treatment of dystonic clenched fist with botulinum toxin. *Mov Disord* 2001;16:907–913.

5. Heinzelmann P, Dow R. Clawhand deformity presumed secondary to Parkinson's disease. *J Hand Surg [Am]* 1985;10:19–21.

6. Gortvai P. Deformities of the hands and feet in parkinsonism and their reversibility by operation. *J Neurol Neurosurg Psychiatry* 1963;26:33–36.

7. Katayama Y, Kasai M, Oshima H et al. Subthalamic nucleus stimulation for Parkinson disease: benefits observed in levodopa-intolerant patients. *J Neurosurg* 2001;95:213–221.

8. Ashour R, Jankovic J. Joint and skeletal deformities in Parkinson's disease, multiple system atrophy, and progressive supranuclear palsy. *Mov Disord* 2006;21:1856–1863.

9. Gowers WR. *A Manual of Diseases of the Nervous System.* Philadelphia: P Blakiston, Son & Co, 1888.

10. Reynolds F, Petropoulous G. Hand deformities in parkinsonism. *J Chronic Dis* 1965;18:593–595.

11. Chou KL, Hurtig HI, Jaggi JL, Baltuch GH. Bilateral subthalamic nucleus deep brain stimulation in a patient with cervical dystonia and essential tremor. *Mov Disord* 2005;20:377–380.

12. Poewe WH, Lees AJ. The pharmacology of foot dystonia in Parkinsonism. *Clin Neuropharmacol* 1987;10:47–56.

13. Künzle H. Bilateral profections from precentral motor cortex to the putamen and other parts of the basal ganglia. An autoradiographic study in *Macaca fascicularis. Brain Res* 1975;88:195–209.

14. Delong MR, Georgopoulos AP, Crucher MD, Mitchell JS, Richardson RT, Alexander GE. Functional organization of the basal ganglia: contributions of single cell recording studies. *Ciba Found Symp* 1984;107:64–82.

15. Gerardin E, Lehericy S, Pochon JB et al. Foot, hand, face and eye representation in the human striatum. *Cereb Cortex* 2003;13:162–169.

16. Thobois S, Dominey P, Frax V et al. Effects of subthalamic nucleus stimulation on actual and imagined movement in Parkinson's disease: a PET study. *J Neurol* 2002;249:1689–1698.

17. Hu MTM, Bland J, Clough C, Ellis CM, Chaudhuri KR. Limb contractures in levodopa-responsive parkinsonism: a clinical and investigational study of seven new cases. *J Neurol* 1999; 246:671–676.

Neuromodulation

Technology at the Neural Interface

VOLUME XI • NUMBER 3 • JULY 2008

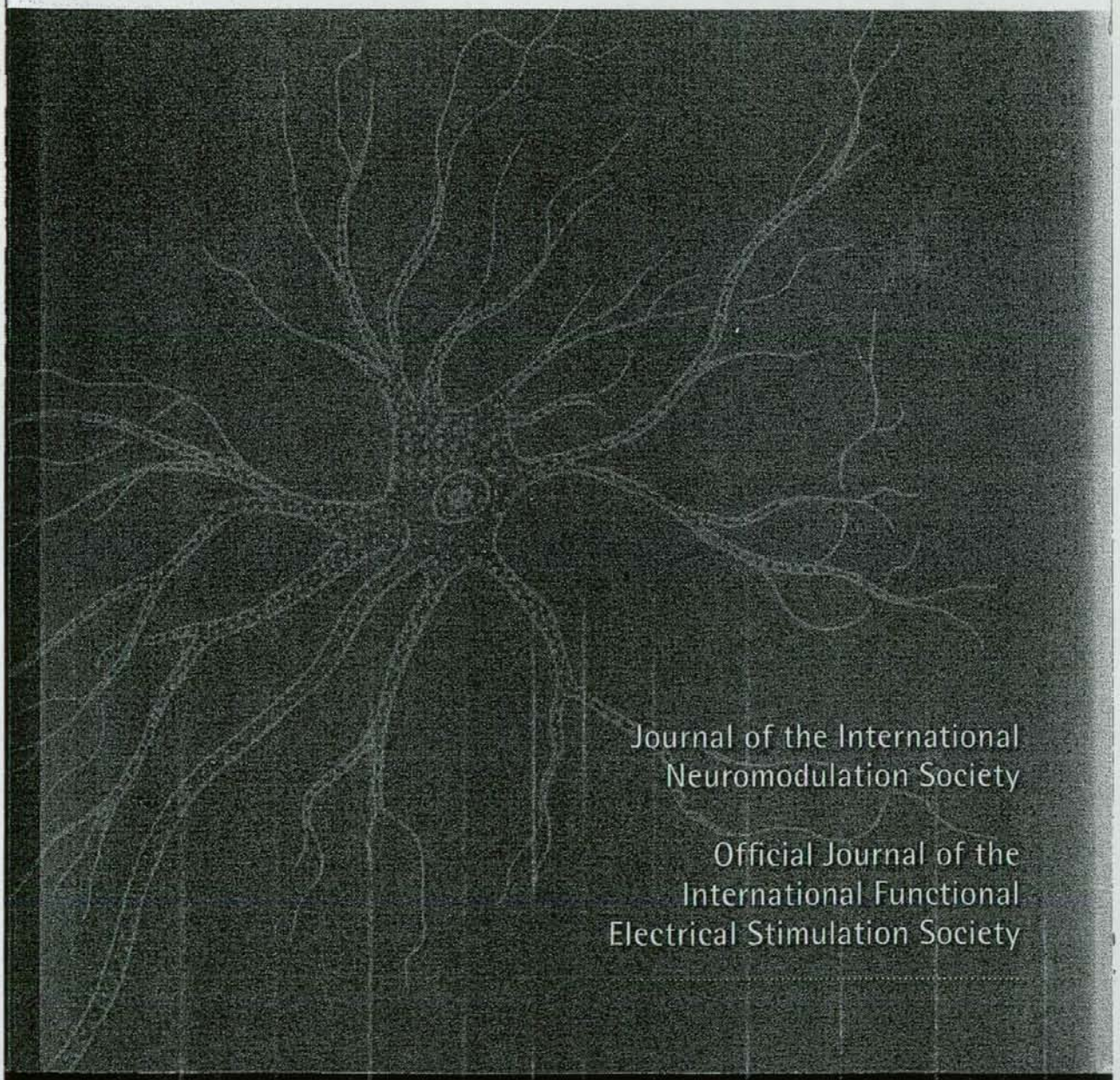

Journal of the International Neuromodulation Society

Official Journal of the International Functional Electrical Stimulation Society

12. Meyerson B. Comments on North RB, Calkins S-K, Campbell DS et al. Automated, patient-interactive, spinal cord stimulator adjustment: a randomized controlled trial. *Neurosurgery* 2003;52:580.

13. Budd K. Spinal cord stimulation: cost-benefit study. *Neuromodulation* 2002;5:75–78.

14. North RB, Kidd D, Shipley J, Taylor RS. Spinal cord stimulation versus reoperation for failed back surgery syndrome: a cost effectiveness and cost utility analysis based on a randomized, controlled trial. *Neurosurgery* 2007;61:361–368; discussion 368–369.

15. Kumar K, Malik S, Demeria D. Treatment of chronic pain with spinal cod stimulation versus alternative therapies: cost-effectiveness analysis. *Neurosurgery* 2002;51:106–111; discussion 115–116.

16. Andrell P, Ekre O, Eliasson T et al. Cost-effectiveness of spinal cord stimulation versus coronary artery bypass grafting pin patients with severe angina pectoris—long-term results from the ESBY study. *Cardiology* 2003;99:20–24.

17. Kemler MA, Furnee CA. Economic evaluation of spinal cord stimulation for chronic reflex sympathetic dystrophy. *Neurology* 2002;59:1203–1209.

Volume 11 • Number 3 • 2008
http://www.blackwell-synergy.com/loi/ner

ORIGINAL ARTICLE

c-Fos Expression After Chronic Electrical Stimulation of Sensorimotor Cortex in Rats

Katsunori Shijo, MD • Yoichi Katayama, MD, PhD • Akiko Yamashita, PhD • Kazutaka Kobayashi, MD, PhD • Hideki Oshima, MD, PhD • Chikashi Fukaya, MD, PhD • Takamitsu Yamamoto, MD, PhD

Department of Neurological Surgery, Nihon University School of Medicine and Division of Applied System Neuroscience, Graduate School of Medical Science, Tokyo, Japan

ABSTRACT

Objectives. Motor cortex stimulation has been used as a treatment for intractable pain. However, the mechanisms underlying its effects remain unclear. In this study, neuroplasticity induced by chronic sensorimotor cortex stimulation was investigated experimentally on the basis of *c-Fos* expression. **Materials and Methods.** The experimental animals employed were adult male Wistar rats. A quadripolar stimulation electrode was positioned over the sensorimotor cortex. We examined the neural activation in response to chronic stimulation using *c-Fos* immunopositivity. **Results.** The results are as follows: 1) *c-Fos* was significantly expressed immediately after the stimulation compared with that in the control; 2) *c-Fos* expression became extensive over the various regions with an increase in stimulation duration; and 3) after two months of stimulation, *c-Fos* was expressed not only on the stimulation side, but also within the contralateral cerebral hemisphere. **Conclusions.** Changes in *c-Fos* expression induced by long-term stimulation indicate the existence of a time-dependent neural plasticity.

KEY WORDS: c-Fos, *motor cortex stimulation, neural plasticity, rat, sensorimotor cortex.*

Introduction

Motor cortex stimulation (MCS) was introduced by Tsubokawa et al. (1) and Katayama et al. (2) as a treatment for intractable thalamic pain. Following their reports, such treatment has been applied to the treatment of peripheral neuropathic pain, and involuntary movements, and very recently to poststroke hemiparesis. Long-term observations have indicated that beneficial effects of chronic MCS can be achieved in many patients with neurologic dysfunction. However, the mechanisms underlying these therapeutic effects have not yet been clarified.

The distribution of neural activity in relation to the motor function is highly dynamic and changes in response to various manipulations, including differential motor training (3–5), the administration of various pharmacologic agents and electrical cortical stimulation (6,7). It is intriguing to speculate that electrical cortex stimulation can cause a functional reorganization and a change in the neurocircuitry. In particular, repeated intracortical microstimulations (6) and kindling (7) have been shown to induce significant motor map expansion in animal experiments.

On the other hand, there are a number of recent studies indicating that gene expression in neurons and glial cells is markedly up-regulated following periods of intense neural activity (8,9). Such stimulation induces a rapid and transient expression of immediate-early genes (IEG) in

Submitted: August 14, 2006; accepted: April 15, 2008. Address correspondence and reprint requests to: Chikashi Fukaya, MD, PhD, Department of Neurological Surgery, Nihon University School of Medicine, Oyaguchi-Kamimachi 30-1, Itabashi-ku, Tokyo 173-8610, JAPAN. Email: chikashi@med.nihon-u.ac.jp

the brain, and the monitoring of IEGs has enabled the visualization of neural plasticity induced by electric stimulation. Many IEGs are transcription factors that directly control the expression of other secondary response genes (10). We investigated the activation of the cortex and related nuclei in response to the chronic electrical stimulation of the sensorimotor cortex using *c-Fos* immunopositivity as a marker of neural activity.

Materials and Methods

This study was carried out in accordance with the Guidelines for Animal Experimentation of the Faculty of Medicine, Nihon University.

Surgical Procedure and Electrical Stimulation

The experimental animals used were 20 adult male Wistar rats (body weight, 300–600 g). The animals were anesthetized for consistency using ketamine hydroxylase (100 mg/kg body weight, intramuscularly) and a mixture of 0.5% epinephrine hydrochloride and lidocaine hydrochloride (1 mL each), injected subcutaneously and below the external ear canals to numb the areas. Then, pentobarbital (Nembutal, Abbott Laboratories, Chicago, IL, USA; 20 mg/kg body weight, intraperitoneally) was injected. After the electrical stimulation parameters were fixed, Nembutal was re-injected.

Each rat was positioned in a stereotactic frame and a cranial burr hole (2 mm × 5 mm) was drilled on the left coronal suture 3.5 mm lateral to the midline (Fig. 1).

A novel quadripolar stimulation electrode (2 mm wide, 5 mm long) was positioned over the sensorimotor cortex. The electrode with four contact points, numbered 0–3 sequentially from the most distal contact 0 to the most proximal contact 3, was placed in such a way that contact 0 was located in the rostral portion of the sensorimotor cortex. Each contact of the electrode was 0.7 mm long; the contacts were 0.7 mm apart.

Anodal pulses were applied at a 25-Hz frequency. The cathode was placed on the caudal side. A stimulation voltage in the range of 2–5 V was applied with an impulse duration of 0.12 msec. The voltage was determined to be less than 80% that required for forelimb muscle contraction. Extension wires were passed from the head to the back subcutaneously and connected to an implantable pulse generator (Soletora Model 7426 IPG, Medtronic Inc., Minneapolis, MN, USA). Stimulation was applied for three hours, two weeks, one month, and two months. Each group consisted of three animals. As control experiments, we carried out the same operative procedures on rats without electrical stimulation and reared the animals for periods matching those for the stimulated rats.

Evaluation of *c-Fos*-Positive Cells

Immunohistochemical analysis was carried out to visualize the localization of *c-Fos*-positive cells within the cerebrum.

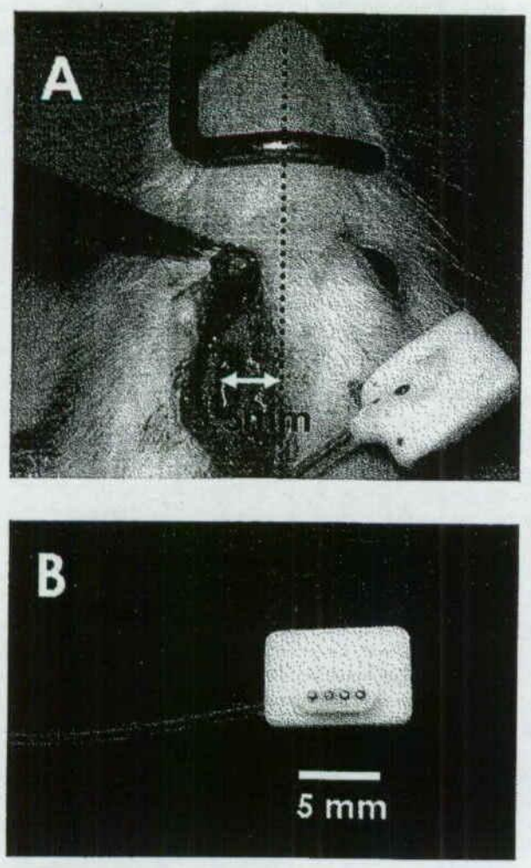

FIGURE 1. Each rat was positioned in a stereotactic frame and a cranial burr hole (2 mm × 5 mm: arrow) was drilled on the left coronal suture 3.5 mm lateral to the midline (A). A novel quadripolar stimulation electrode (2 mm wide, 5 mm long) was positioned over the sensorimotor cortex. Each contact of the electrode was 0.7 mm long; the contacts were 0.7 mm apart (B).

After the stimulation, the rats were killed by administering intraperitoneal pentobarbital (60 mg/kg body weight) and perfusing them with 4% paraformaldehyde in 0.1 M phosphate-buffered saline (pH 7.4). The extracted brains were postfixed in the same fixative for 12 hours with constant shaking, and then successively immersed in 10% and 20% sucrose for approximately 48 hours each at 4° until the brains were settled at the bottom of the solution. The brains were embedded in an optimal cutting temperature compound, frozen, and sectioned (40 µm thick) on a sliding microtome.

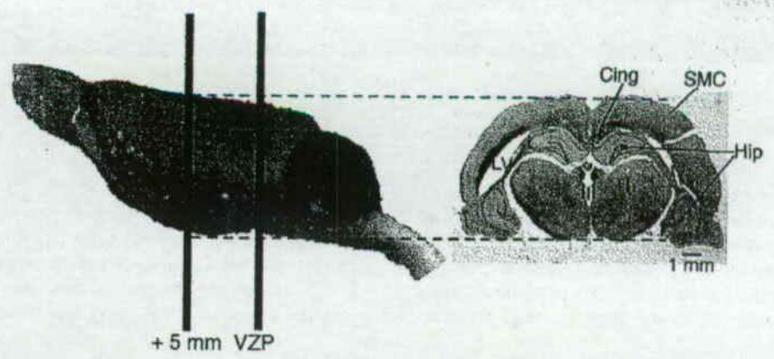

FIGURE 2. A parallel slice was made about 5 mm anterior to the VZP (vertical zero plane), which just included the stimulated part of the sensorimotor cortex. SMC, sensorimotor cortex; Th, thalamus; Cing, cingulate gyrus; Hip, hippocampus; III, third ventricle; LV, lateral ventricle; cc, corpus callosum. Bar = 1 mm.

Free-floating sections for *c-Fos* immunohistochemical analysis were pretreated with 0.3% H_2O_2 in methanol for 30 min and incubated in 1% normal goat serum and 10% fish gelatin in phosphate buffer (FG-PB, pH 7.4) for 30 min. They were then reacted with sheep anti-*c-Fos* antiserum (diluted 1 : 2000 in FG-PB, Chemicon, Temecula, CA, USA) for 48 hours in a refrigerator with constant shaking. After several washes with PB, the sections were reacted with a goat anti-sheep immunoglobulin G (IgG) secondary antibody (Vectastain ABC Elite kit, Vector Laboratories, Burlingame, CA, USA) for two hours at room temperature. Next, the sections were incubated with ABC solution (ABC kit) and reacted with 0.02% 3,3'-diaminobenzidine and 0.03% H_2O_2 for 10 min. Some selected sections were stained with neutral red for counterstaining. Neighboring sections were stained by conventional Nissl staining employing crystal violet. The sections were mounted on gelatin-coated glass slides, air-dried, dehydrated in ethanol, cleared in xylene and coverslipped (Fig. 2).

The sections were observed and photographed using a Coolscope CCD camera (Nikon, Tokyo, Japan) attached to an Eclipse microscope (Nikon). High magnification photographs were constructed employing picture processing software ACT1 (Nikon). The distribution of *c-Fos*-positive cells was plotted using a Neurolucida system (MicroBrightField, Williston, VT, USA) installed on a personal computer attached to an AX-10 microscope (Olympus, Tokyo, Japan) and a 2400c CCD camera (Hamamatsu Photonics, Hamamatsu, Japan).

Types of *c-Fos*-Immunoreactive Cell

To confirm cell type, we also used fluorescence double-staining. Ionized calcium-binding adaptor molecule 1 (Iba1) was used as a marker of microglia/macrophages (11), the glial fibrillary acidic protein (GFAP) was used as a marker of astrocytes, and neuron-specific enolase (NSE) and microtubule-associated protein 2 (MAP2) were used as markers of neurons. Selected sections were pretreated with 0.3% hydrogen peroxide in methanol and incubated in normal goat/horse/donkey serum and FG-PB (pH, 7.4). Then, the sections were incubated for 48 hours at 4° with anti-Iba1 rabbit antiserum (Wako, Osaka, Japan; final dilution of 1 : 200) or an anti-GFAP (Chemicon; 1 : 100) mouse antibody or an anti-NSE mouse antibody (Laboratory Vision Corporation, Fremont, CA, USA; 1 : 1000) diluted in FG-PB.

To visualize the immunoreactive sites, the sections were reacted with diaminobenzidine (DAB) and hydrogen peroxide solution. After treatment with an ABC blocking kit (Vector), the sections were reacted with an anti-*c-Fos* sheep antibody, as mentioned above, and hydrogen peroxide solution with cobalt chloride was used for visualization. For immunofluoresence study, some of the sections were incubated for 48 hours at 4° with a mixture of anti-*c-Fos* sheep antiserum and an anti-MAP2 mouse antibody (Sigma, St. Louis, MO, USA; 1 : 2000) diluted in FG-PB. The sections were reacted with a cocktail of secondary antibodies: a rhodamine-labeled anti-mouse IgG horse antibody (Vector) and an fluorescein isothiocyanate-labeled anti-sheep IgG donkey antibody (Chemicon). The sections were set on a glass slide and mounted in nonfluorescent glycerine (Merck, Darmstadt, Germany).

Detection of Degenerating Neurons

To detect degenerating neurons, Fluoro-Jade B (FJB) staining was carried out in accordance with the method of Schmued et al. (12). The sections were treated with 1% sodium hydroxide in 80% ethanol for 5 min and in 0.06% potassium permanganate for 10 min on a shaker. They

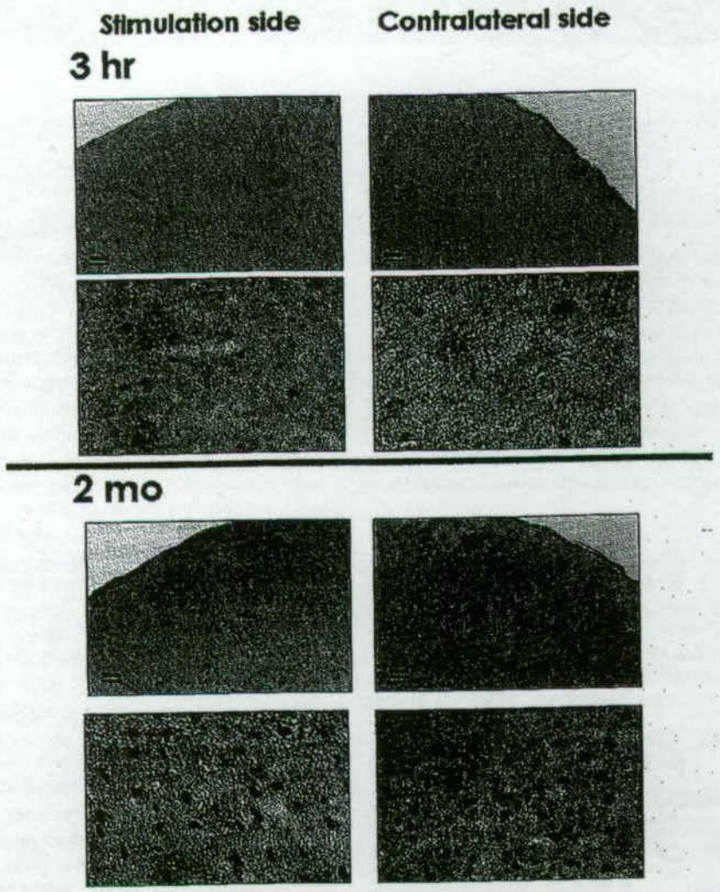

FIGURE 3. c-*Fos*-immunopositive cells observed microscopically in sensorimotor cortex on sides ipsilateral and contralateral to stimulation for three hours and two months of stimulation. Bars = above, 100 μm; below, 20 μm.

were then incubated in freshly mixed 0.0004% FJB (Cosmobio, Tokyo, Japan) in 0.1% acetic acid for 20 min, washed in distilled water and air-dried at 50° for 10 min. The sections were cleaned using xylene and coverslipped.

Results

In the sensorimotor cortex, few FJB-positive cells were observed for all experimental periods, indicating that no cell death was induced by the electrical stimulation in this study (data not shown). Moreover, only small numbers of *c-Fos*-positive cells were detected in the surgically operated control animals without stimulation, showing that *c-Fos* is mostly activated by the electrical stimulation. Compared with that in the control animals, a high density of *c-Fos*-immunopositive cells was observed in the rats subjected to three hours to two months of electrical stimulation of the sensorimotor cortex. Because the immunopositivity for *c-Fos* was found to be perinuclear in the cells, it was difficult to determine whether the immunopositive cells were neurons or glia. In the white matter and corpus callosum, observed *c-Fos*-immunopositive cells less than 10 μm in diameter indicated that at least some of the *c-Fos*-immunopositive cells were glia. On the other hand, in the gray matter, *c-Fos*-immunopositive cells with large somata also were (more than 20 μm in diameter) observed (Fig. 3). In the cortical gray matter, NSE/MAP2 and *c-Fos* double-stained cells were observed (Fig. 4A and B, respectively), indicating that this IEG is expressed in the neuronal cells in the cortex. On

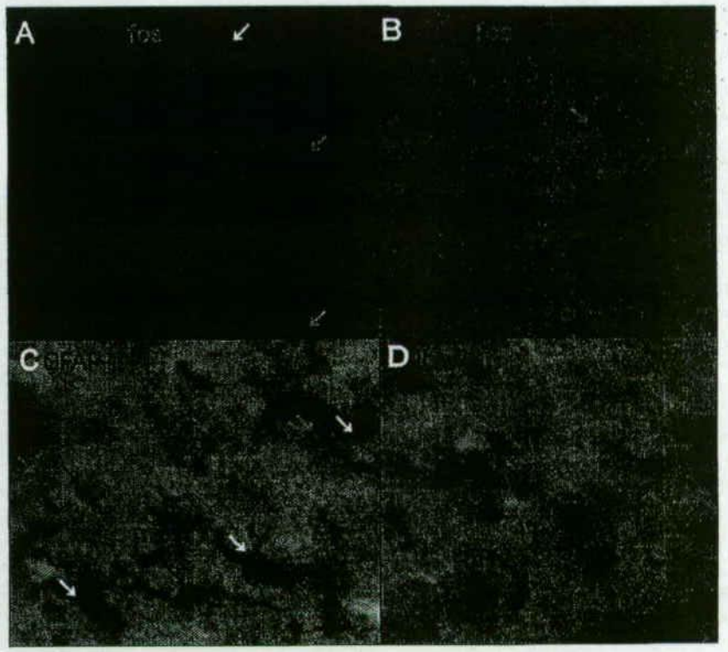

FIGURE 4. In layers II/III of the motor cortex after two months stimulation, MAP2-positive cells showed *c-Fos* immunoreactivity (yellow arrow). There were also MAP2-positive/*c-Fos*-negative neurons (red arrow) were also observed. MAP2 (green arrows in A) or neuron-specific enolase (NSE)-negative (blue arrow in B)/*c-Fos*-positive cells also were observed, suggesting that astrocytes also express *c-Fos*. At the border between the gray matter of the motor cortex and the white matter, glial fibrillary acidic protein (GFAP)-positive/*c-Fos*-positive (yellow arrows in C), GFAP-positive/*c-Fos*-negative (black arrows) and GFAP-negative/*c-Fos*-positive (blue arrows) cells were observed, indicating that both neurons and astrocytes express *c-Fos*. We detected no Iba1-positive cells showing *c-Fos* immunoreactivity (D). Bars = 20 μm.

TABLE 1. Numbers of *c-Fos*-Immunopositive Cells After Stimulation

		Nonstimulation $N=3$	3 Hours $N=3$	2 Weeks $N=3$	1 Month $N=3$	2 Months $N=3$
SMC	I	37.00 ± 22.91	148.67 ± 139.01	170.33 ± 59.68*	111.75 ± 41.55*	165.67 ± 88.23*
	C	35.67 ± 19.60	56.33 ± 40.50	92.33 ± 38.32*	92.00 ± 38.32*	193.00 ± 107.59*
Th	I	14.67 ± 12.74	112.67 ± 77.02*	113.67 ± 60.62*	91.00 ± 66.15*	134.00 ± 91.33*
	C	25.67 ± 9.81	75.67 ± 52.69	49.00 ± 22.61	118.50 ± 52.82*	197.33 ± 92.12*
Cing	I	41.67 ± 40.50	85.33 ± 15.01	150.67 ± 109.35	84.50 ± 64.26	108.33 ± 86.33
	C	21.33 ± 17.04	53.67 ± 25.58	103.33 ± 108.65	91.75 ± 51.10*	186.67 ± 84.03*

Asterisks, significantly different from nonstimulation; *$p < 0.05$, Mann–Whitney *U*-test.
SMC, sensorimotor cortex; Th, thalamus; Cing, cingulate gyrus; I, side ipsilateral to stimulation; C, side contralateral to stimulation.

the other hand, both GFAP-negative (blue arrows in Fig. 4C) and GFAP-positive cells (yellow arrows, Fig. 4C) expressing *c-Fos* immunoreactivity were observed, indicating that both neurons and astrocytes show the transcription of a new gene. No Iba1 and *c-Fos* double-stained cells were detected (Fig. 4D). We concluded, therefore, that both neurons and glia are *c-Fos*-immunopositive.

The distribution pattern of *c-Fos*-immunopositive cells is summarized in Table 1. It changed significantly depending on stimulation duration (Mann–Whitney *U*-test).

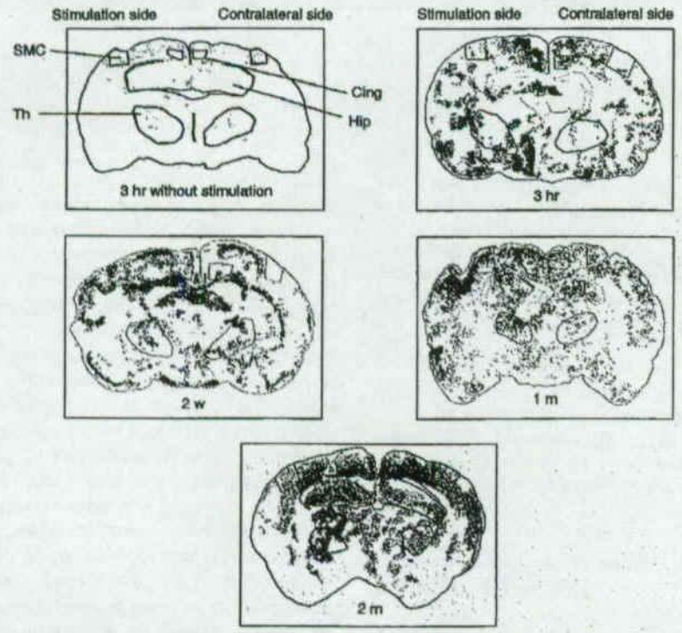

FIGURE 5. Distributions of *c-Fos*-immunopositive cells in coronal sections that contain the stimulation site after three hours without stimulation, and after three hours, two weeks, one month, and two months of stimulation. The dots indicate immunopositive cells on the ipsilateral and contralateral sides to the stimulation. The density of *c-Fos*-immunopositive cells changed gradually from three hours to two months. SMC, sensorimotor cortex; Th, thalamus; Cing, cingulate gyrus; Hip, hippocampus.

Figure 5 shows the distribution of *c-Fos*-immunopositive cells in coronal sections from a control animal and from rats after three hours, two weeks, and two months of stimulation. After three hours of stimulation, higher densities of *c-Fos*-immunopositive cells were found in the dentate gyrus, thalamus, and medial amygdala on the side ipsilateral to the electrical stimulation than in the same areas on the contralateral side. Immunopositivity also was observed in the piriform cortex, hippocampus, and striatum of both hemispheres. After two weeks of stimulation, higher densities of *c-Fos*-immunopositive cells were found in the neocortex, hippocampus, dentate gyrus, fimbria, corpus callosum, ventral premaxillary nucleus, and hypothalamus of both hemispheres. *c-Fos*-immunopositive cells also were noted in the reticular nucleus of the thalamus of the contralateral cerebrum. After one month of stimulation, higher densities of *c-Fos*-immunopositive cells were found in the neocortex, hippocampus, dentate gyrus, fimbria, and corpus callosum of both hemispheres, and in the thalamus of the contralateral hemisphere. After two months of stimulation, higher densities of *c-Fos*-immunopositive cells were found in the hippocampus, thalamus, and corpus callosum on both sides.

To evaluate the changes in *c-Fos* expression level in each hemisphere, we compared cell density between the ipsi- and contralateral sides. The *c-Fos*-immunopositive cell ratios for the contra- and ipsilateral sides of stimulation were calculated (Fig. 6). At the early stage, higher densities of *c-Fos*-immunopositive cells were observed in the sensorimotor cortex, cingulate gyrus, and thalamus on the stimulation side. However, *c-Fos* expression level began to increase slightly in the sensorimotor cortex on the opposite side after two weeks of stimulation. The expression of *c-Fos* in the sensorimotor cortex on the contralateral side after one month of stimulation was enhanced. At this point, *c-Fos* expression extended to the thalamic nucleus and cingulate cortex on both sides. After two months, a higher density of *c-Fos*-immunopositive cells was observed on the side contralateral to the stimulation.

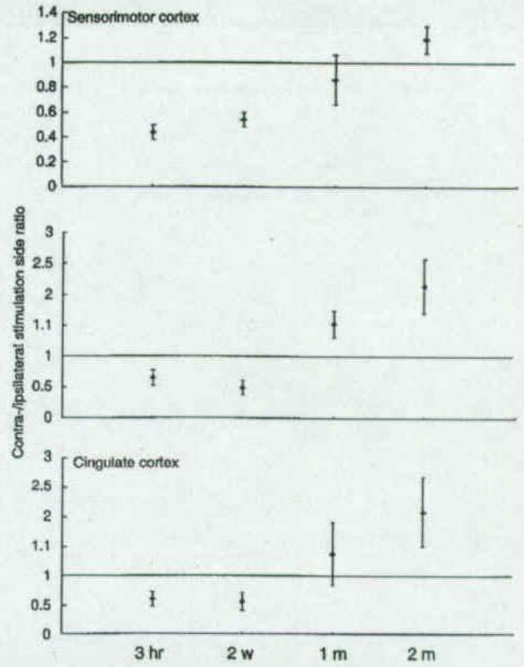

FIGURE 6. Cell densities on ipsilateral and contralateral sides compared in terms of positive cell ratios for contralateral/ipsilateral sides to stimulation in sensorimotor cortex (A), cingulate cortex (B), and thalamus (C). At the early stage, higher densities of *c-Fos*-immunopositive cells were observed on the stimulated side. However, after two months, higher densities of *c-Fos*-immunopositive cells were noted on the side contralateral to the stimulation.

Discussion

The use of chronic MCS as a treatment for medically refractory deafferentation pain, mainly thalamic pain, was initiated by Tsubokawa et al. and Katayama et al. (1,2). Katayama et al. reported excellent or good control of pain (pain reduction > 60%) in about 50% of patients employing this therapeutic technique for follow-up periods of more than two years (2). More recently, this procedure has been used as a treatment for movement disorders, including Parkinson's disease (13,14) and poststroke involuntary movement (15–17). Katayama et al. speculated that the therapeutic effects on involuntary movements are related to the desynchronization of abnormal activities that are transmitted to the corticospinal tract (17). Such an abnormal distribution of neural activity and the constitution of the neural network associated with the sensorimotor function could change in response to chronic MCS.

We examined the *c-Fos* expression after the long-term chronic electrical stimulation of the sensorimotor cortex in rats. It has been reported that epileptic seizures can induce high *c-Fos* expression levels in various areas of the brain in animals. Morgan et al. first described a marked and specific induction of *c-Fos* in an identifiable population of what *in vivo* following metrazol-induced seizures in mice (18). Doi et al. also found that electroconvulsive therapy induces a strong *c-Fos* expression in all regions of the brain except the thalamus (19).

In this study, the *c-Fos* expression induced by chronic sensorimotor cortex stimulation demonstrated the functional activation of several cortical and deep brain structures, mainly the sensorimotor cortex, thalamus, hippocampus, and cingulate gyrus. This pattern of *c-Fos* expression differed from that observed after epileptic seizures in previous studies (18,19). In addition, we observed no convulsions or seizurelike symptoms during chronic stimulation in any of our rats. Voskuyl et al. have described in detail the threshold of electrical stimulation that induces convulsions (20). According to their experimental study employing nonanesthetized rats, the conditions of approximately 1.3 μA with a 2-msec duration and a 50-Hz frequency represent the threshold for convulsions in rats. The stimulation parameters used in our study were a 0.12-msec duration, a 25-Hz frequency and an intensity that was 80% the threshold for muscle contraction (approximately 2–3 V). Thus, convulsive seizures could hardly have occurred during the chronic sensorimotor cortex stimulation in this study.

It also was confirmed that degenerating neurons are absent in the sensorimotor cortex immediately below the stimulation electrode, as determined by the FJB histochemical staining technique (12). The *c-Fos* expression observed in this study was therefore almost completely induced by the electrical stimulation of the sensorimotor cortex without the induction of epileptic seizures or neuronal degeneration.

Several experimental studies of the distribution of *c-Fos* expression after electrical or magnetic cortical stimulation have been conducted. Sagar et al. stimulated the rat sensorimotor cortex electrically and examined *c-Fos* expression immunohistochemically. Three hours after the start of stimulation, focal nuclear *c-Fos* staining was observed in the sensorimotor cortex and thalamus, pontine nucleus, globus pallidus, and cerebellum (21). Viltart and Sequeira also stimulated the rat sensorimotor cortex for one hour and observed catecholaminergic neuronal activity. Their data suggest that the stimulation of the sensorimotor cortex preferentially activates catecholaminergic neurons of the rostral ventrolateral medulla (22).

On the other hand, certain studies have shown experimental studies using transcranial magnetic stimulation (TMS). Hausmann et al. demonstrated a marked increase

in *c-Fos* expression level in neurons of the parietal cortex and in a few scattered neurons of the hippocampus of rats after chronic repetitive TMS for 14 days (23). According to an experimental study by Doi et al., six TMS sessions induce widespread nuclear *c-Fos*-like immunopositivities in the frontal cortex, lateral orbital cortex, striatum, lateral septal nucleus, piriform cortex, dentate gyrus, and Ammon's horn among other structures. These reactivities were greater than those for two TMS sessions (19). Various affected portions of the brain and patterns of *c-Fos* expression after cortical stimulation were noted in the above-mentioned studies. The results obtained basically agree with each other and with our results for short-term stimulation. However, *c-Fos* expression and its changes were monitored for only a short period in all the previous studies. Even in that using daily repetitive TMS, the maximum period of *c-Fos* expression observation was two weeks. To the best of out knowledge, this is the first experimental study in which *c-Fos* expression and its changes on sensorimotor cortex stimulation have been observed for two months.

The most important results obtained in this study can be summarized as follows:

1. *c-Fos* was significantly expressed immediately after the sensorimotor cortex stimulation as compared with that in the control.
2. Such *c-Fos* expression changed with time. It generally became extended over the cerebral cortex and deep brain structures with an increase in stimulation duration.
3. *c-Fos* expression was noted not only on the stimulation side, but also on the contralateral side. After two months, a higher density of *c-Fos*-immunopositive cells was observed on the side contralateral to the stimulation than on the stimulation side.

Animal and human research over the recent decades has provided increasing evidence of the brain's capacity for reorganizing its neural networks to adapt to environmental needs. From the basis of the results of this study, functional modulation as demonstrated by *c-Fos* expression suggests the existence of MCS-induced neural plasticity that intensifies with the stimulation duration.

The *c-Fos* expression after continuous cortical stimulation was noted not only on the side ipsilateral to the stimulation but also on the contralateral side. Several clinical observations appear to support this phenomenon. In our clinical experience, gradual improvements of gait have sometimes been observed after long-term MCS in patients with post-stroke motor deficit. Canavero and Bonicalzi reported the effects of bilateral MCS on plegic stroke rehabilitation. They stated that MCS can modestly boost the rehabilitation effects in chronic stroke patients, with effects differing between ipsilateral and contralateral stimulations (24). These findings appear to support the beneficial effects of long-term MCS of the contralateral cerebral hemisphere. Further research is needed to elucidate the mechanism underlying the predominant effect of the long-term stimulation of the contralateral side.

It has been speculated that the construction of an abnormal network in the upper central nervous system above a deafferentation site is associated with the mechanism of deafferentation pain onset (1,2,16). MCS could exert neuroplastic effects for coping with such an abnormal network. This characteristic of MCS, that is the induction of neural plasticity, may be useful for the application of MCS as a therapeutic method for other functional diseases. In fact, MCS is increasingly employed as a therapeutic method for various movement disorders and poststroke motor dysfunction. Its therapeutic indications should gradually expand owing to its unique ability to elicit neural plasticity.

Conclusions

Chronic sensorimotor cortex stimulation induced *c-Fos* expression, and the affected areas expanded, including the side contralateral to the stimulation, in association with stimulation duration. Such results indicate the existence of a high degree of neural plasticity in the brain induced by chronic sensorimotor cortex stimulation. Furthermore, on the basis of these results, it is speculated that chronic MCS modulates abnormal neural networks that develop in patients with deafferentation pain. This therapeutic method should be adopted as a treatment for various functional diseases involving with abnormal neural reconstruction.

Acknowledgment

This work was supported by a Grant-in-Aid for Scientific Research (A18209046 and C17591535) from the Ministry of Education, Culture, Sports, Science, and Technology of Japan.

Conflict of Interest

The authors reported no conflict of interest.

References

1. Tsubokawa T, Katayama Y, Yamamoto T, Hirayama T, Koyama S. Chronic motor cortex stimulation in patients with thalamic pain. *J Neurosurg* 1993;78:393–401.

2. Katayama Y, Fukaya C, Yamamoto T. Poststroke pain control by chronic motor cortex stimulation: neurological characteristics predicting a favorable response. *J Neurosurg* 1998;89:585–591.

3. Conner JM, Culberson A, Packowski C, Chiba AA, Tuszynski MH. Lesions of the basal forebrain cholinergic system impair task acquisition and abolish cortical plasticity associated with motor skill learning. *Neuron* 2003;38:819–829.

4. Kleim JA, Barbay S, Nudo RJ. Functional reorganization of the rat motor cortex following motor skill learning. *J Neurophysiol* 1998;80:3321–3325.

5. Nudo RJ, Wise BM, SiFuentes F, Milliken GW. Neural substrates for the effects of rehabilitative training on motor recovery after ischemic infarct. *Science* 1996;272:1791–1794.

6. Nudo RJ, Jenkins WM, Merzenich MM. Repetitive microstimulation alters the cortical representation of movements in adult rats. *Somatosens Mot Res* 1990;7:463–483.

7. Teskey GC, Monfils MH, VandenBerg PM, Kleim JA. Motor map expansion following repeated cortical and limbic seizures is related to synaptic potentiation. *Cereb Cortex* 2002;12:98–105.

8. Herrera DG, Robertson HA. Activation of *c-fos* in the brain. *Prog Neurobiol* 1996;50:83–107.

9. Reddington M, Priller J, Treichel J, Haas C, Kreutzberg GW. Astrocytes and microglia as potential targets for calcitonin gene related peptide in the central nervous system. *Can J Physiol Pharmacol* 1995;73:1047–1049.

10. Fujiki M, Steward O. High frequency transcranial magnetic stimulation mimics the effects of ECS in upregulating astroglial gene expression in the murine CNS. *Brain Res Mol Brain Res* 1997;44:301–308.

11. Ito D, Imai Y, Ohsawa K, Nakajima K, Fukuuchi Y, Kohsaka S. Microglia-specific localisation of a novel calcium birding protein, Iba1. *Brain Res Mol Brain Res* 1998;57:1–9.

12. Schmued LC, Albertson C, Slikker W Jr. Fluoro-Jade: a novel fluorochrome for the sensitive and reliable histochemical localization of neuronal degeneration. *Brain Res* 1997;751:37–46.

13. Canavero S, Bonicalzi V, Paolotti R et al. Therapeutic extradural cortical stimulation for movement disorders: a review. *Neurol Res* 2003;25:118–122.

14. Pagni CA, Altibrandi MG, Bentivoglio A et al. Extradural motor cortex stimulation (EMCS) for Parkinson's disease: history and first results by the Study Group of the Italian Neurosurgical Society. *Acta Neurochir Suppl* 2005;93:113–119.

15. Franzini A, Ferroli P, Leone M, Broggi G. Stimulation of the posterior hypothalamus for treatment of chronic intractable cluster headaches: first reported series. *Neurosurgery* 2003;52:1095–1099.

16. Katayama Y, Yamamoto T, Kobayashi K, Kasai M, Oshima H, Fukaya C. Motor cortex stimulation for post-stroke pain: comparison of spinal cord and thalamic stimulation. *Stereotact Funct Neurosurg* 2001;77:183–186.

17. Katayama Y, Yamamoto T, Kobayashi K, Oshima H, Fukaya C. Deep brain and motor cortex stimulation for post-stroke movement disorders and post-stroke pain. *Acta Neurochir Suppl* 2003;87:121–123.

18. Morgan JI, Cohen DR, Hempstead JL, Curran T. Mapping patterns of *c-fos* expression in the central nervous system after seizure. *Science* 1987;237:192–197.

19. Doi W, Sato D, Fukuzako H, Takigawa M. *c-Fos* expression in rat brain after repetitive transcranial magnetic stimulation. *Neuroreport* 2001;12:1307–1310.

20. Voskuyl RA, Dingemanse J, Danhof M. Determination of the threshold for convulsions by direct cortical stimulation. *Epilepsy Res* 1989;3:120–129.

21. Sagar SM, Sharp FR, Curran T. Expression of *c-fos* protein in brain: metabolic mapping at the cellular level. *Science* 1988;240:1328–1331.

22. Viltart O, Sequeira H. Induction of *c-fos*-like protein in bulbar catecholaminergic neurones by electrical stimulation of the sensorimotor cortex in the rat. *Neurosci Lett* 1999;260:65–68.

23. Hausmann A, Weis C, Marksteiner J, Hinterhuber H, Humpel C. Chronic repetitive transcranial magnetic stimulation enhances *c-fos* in the parietal cortex and hippocampus. *Brain Res Mol Brain Res* 2000;76:355–362.

24. Canavero S, Bonicalzi V. Transcranial magnetic stimulation for central pain. *Curr Pain Headache Rep* 2005;9:87–89.

Neuromodulation

Technology at the Neural Interface

VOLUME X • NUMBER 3 • JULY 2007

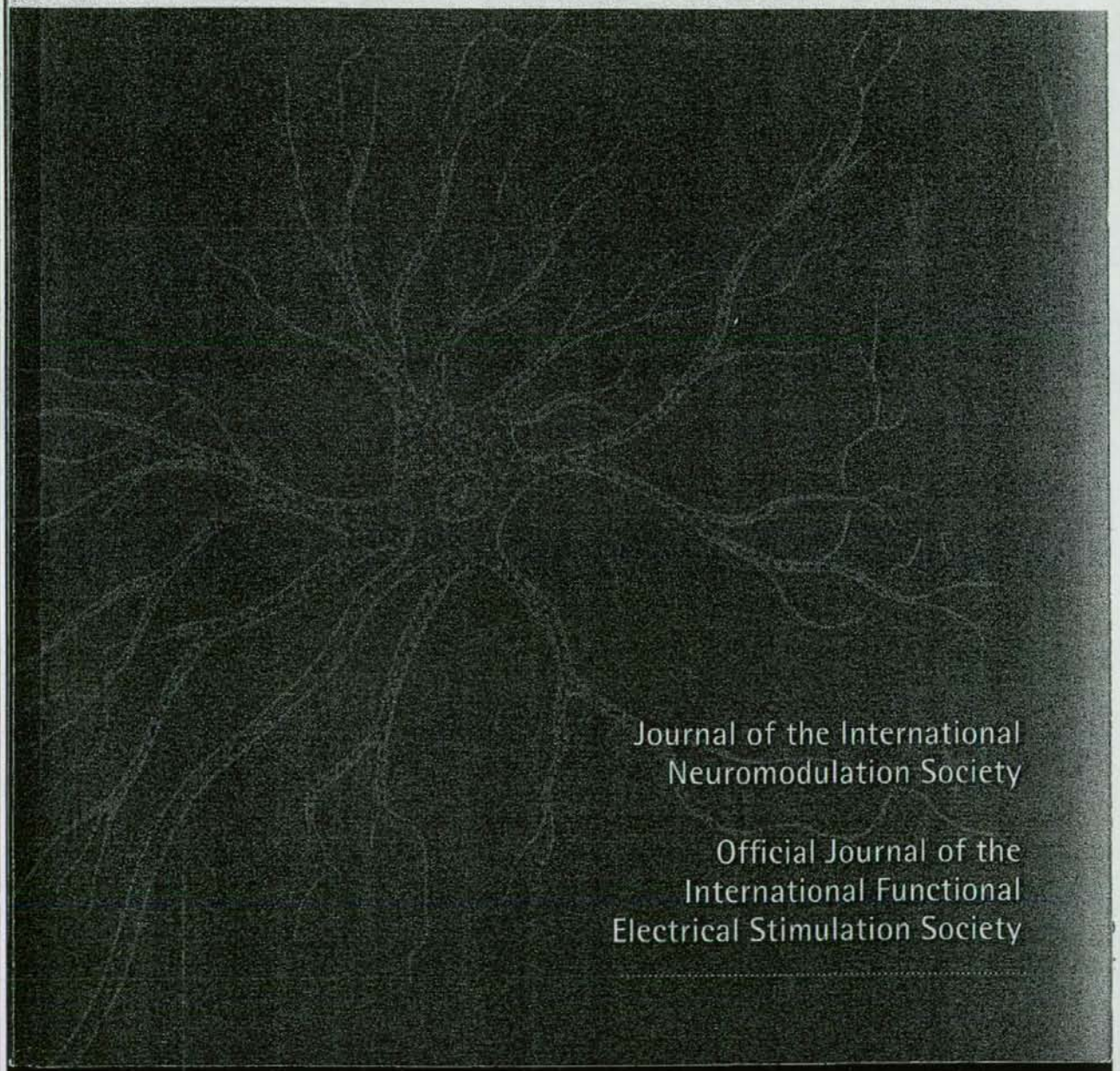

Journal of the International Neuromodulation Society

Official Journal of the International Functional Electrical Stimulation Society

NEUROMODULATION: TECHNOLOGY AT THE NEURAL INTERFACE

Volume 10 • Number 3 • 2007
http://www.blackwell-synergy.com/loi/ner

ORIGINAL ARTICLE

Changes in Glucose Metabolism in Cerebral Cortex and Cerebellum Correlate With Tremor and Rigidity Control by Subthalamic Nucleus Stimulation in Parkinson's Disease: A Positron Emission Tomography Study

Takafumi Nagaoka, MD, PhD • Yoichi Katayama, MD, PhD • Toshikazu Kano, MD, PhD • Kazutaka Kobayashi, MD, PhD • Hideki Oshima, MD, PhD • Chikashi Fukaya, MD, PhD • Takamitsu Yamamoto, MD, PhD

Department of Neurological Surgery, Division of Applied System Neuroscience, Nihon University School of Medicine, Tokyo, Japan

ABSTRACT

Objective. Employing [^{18}F]fluorodeoxyglucose (FDG) positron emission tomography (PET) to assess the correlation between the effect of deep brain stimulation (DBS) on the subthalamic nucleus (STN) and the regional cerebral metabolic rate of glucose (rCMRGlc) in advanced Parkinson's disease patients ($N=8$). **Materials and Methods.** On the basis of patients' diary records, we performed FDG-PET during the off-period of motor activity with on- or off-stimulation by STN-DBS on separate days and analyzed the correlation between changes in motor symptoms and alterations in the rCMRGlc. **Result.** When FDG-PET was performed, the motor score on the unified Parkinson's disease rating scale (UPDRS) was 64% lower with on-stimulation than with off-stimulation ($p < 0.001$, Wilcoxon single-rank test). STN-DBS increased the rCMRGlc in the posterior part of the right middle frontal gyrus, which corresponded to the premotor area, and the right anterior lobe of the cerebellum ($p < 0.005$, paired t-test). No region exhibited a decrease in rCMRGlc. Among the items of the UPDRS motor score, the changes in resting tremor and rigidity of the left extremities showed a significant correlation with the changes in rCMRGlc observed in the right premotor area ($p < 0.02$ and $p < 0.05$, respectively, Spearman's rank correlation). **Conclusions.** STN-DBS either activates the premotor area or normalizes the deactivation of the premotor area. These FDG-PET findings obtained are consistent with the idea that STN-DBS modifies the activities of neural circuits involved in motor control.

KEY WORDS: *Deep brain stimulation, FDG-PET, Parkinson's disease, subthalamic nucleus.*

Submitted: July 25, 2006; accepted: April 2, 2007. Address correspondence and reprint requests to: Takamitsu Yamamoto, MD, PhD, Department of Neurological Surgery, Nihon University School of Medicine, 30-1, Ohyaguchi, Kamimachi, Itabashi-ku, Tokyo 173-8610, JAPAN. Email: nusmyama@med.nihon-u.ac.jp

Introduction

Recent clinical studies have demonstrated that deep brain stimulation (DBS) of the subthalamic nucleus (STN) affords great benefits to the daily activities of patients with advanced Parkinson's disease (PD) (1–7), and lowers the requirement for levodopa (or an equivalent medication) (3,8). In most of these studies, the major effects of STN stimulation were observed during the off-period or off-medication (1–8).

The mechanism(s) underlying these neurologic improvements induced by STN-DBS has been investigated by positron emission tomography (PET) employing [^{15}O]H_2O or [^{18}F]fluorodeoxyglucose (FDG), reflecting regional cerebral activity. Previous PET studies (9–15) have demonstrated that STN-DBS increases activity of the supplementary motor area, the premotor area, the dorsolateral prefrontal cortex, or the anterior cingulate gyrus during the execution of motor tasks or at rest.

However, little is yet known concerning the relationship of changes in regional cerebral activity induced by STN-DBS to improvement of motor symptoms. In this study, we analyzed the correlation between changes in motor symptoms and alterations in the regional cerebral metabolic rate of glucose (rCMRGlc) using FDG-PET, which provides information on changes in the regional cerebral activity (16).

Clinical Materials and Methods

Patient Population and Protocol

This study was approved by the Institutional Review Board of Nihon University Hospital and Nishidai Clinic, and written consent was obtained from each subject after a detailed explanation of the procedures had been given. We studied eight patients with advanced idiopathic PD (four men and four women; mean age: 61.9 ± 11.1 years). The patients in this study were referred to us by neurologists specializing in the treatment of PD. The effects of various combinations of medical therapies were examined by the referring neurologists. All patients responded well to levodopa, but showed severe motor fluctuations. Using the Hoehn and Yahr disability scale to assess levels of disability, all patients were at Stages 3, 4, or 5 during off-periods and Stages 1, 2, or 2.5 during on-periods. In this article, we use "off-period" to indicate the bad period of daily fluctuations in motor symptoms and "on-period" to indicate the good period of daily fluctuation in motor symptoms.

There were two reasons why these patients had become disabled despite having adequate responses to levodopa:

1. Severe fluctuations in motor symptoms occurred, with or without levodopa-induced dyskinesia, in five cases.
2. Sufficient doses of levodopa-induced side-effects, which included nausea and vomiting, arrhythmia, orthostatic hypotension, and psychiatric symptoms, in three cases.

The dose of medication, expressed in this article, is the levodopa-equivalent dose (LED) (17) (the regular dose of levodopa plus carbidopa [or benserazide] + 0.75 × the dose of controlled-release levodopa plus carbidopa + 10 × the dose of bromocriptine + 100 × the dose of pergolide) and the total dose of monoamine oxidase B (MAO-B) inhibitor (selegiline).

Patient's Diary for Advanced PD

We employed a patient's diary to assess the patterns of motor fluctuations and the durations of the on- and off-periods over the whole day (Fig. 1). This diary included items for medication and motor symptoms. Motor function was evaluated according to a four-point rating scale: 1) almost normal; 2) moderately disabled; 3) markedly disabled; and 4) severely disabled. The patients evaluated these items and recorded the results by themselves at one-hour intervals. Based on this record, the on- and off-periods of daily fluctuations in motor symptoms were determined for each patient.

Surgical Procedures Performed

A Leksell series G head frame (Elekta Instruments AB, Stockholm, Sweden) was fixed to the

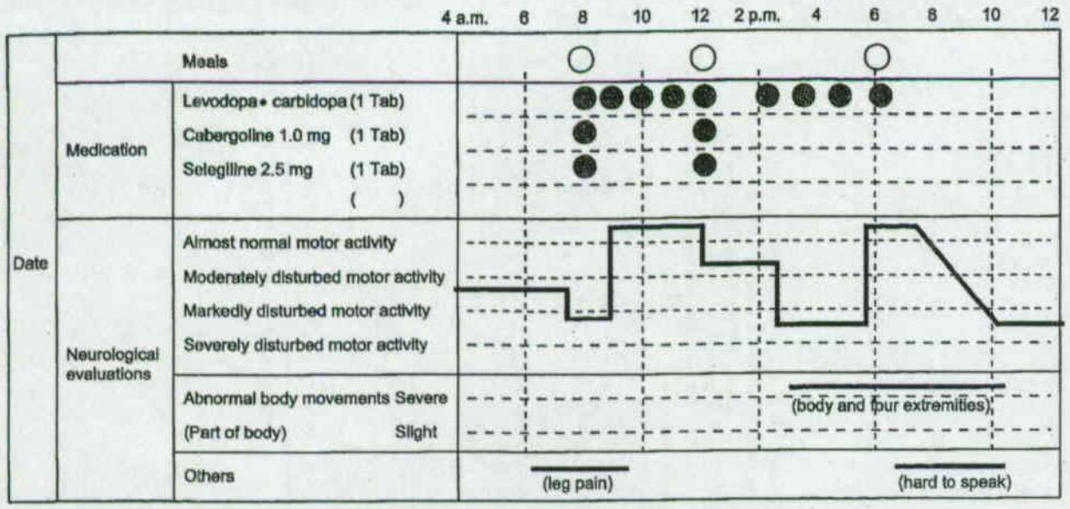

FIGURE 1. Patient's diary. Patients recorded their medication and motor function by themselves at one-hour intervals. This diary was used for estimating the patterns of motor fluctuations and the durations of the on- and off-periods.

skull. Magnetic resonance (MR) imaging was carried out at a 1-mm slice thickness, and the anterior commissure (AC) and posterior commissure (PC) were identified using specialized software (Leksell SurgiPlan, Elekta). An X-ray indicator also was employed to identify the AC and PC on plain X-ray photographs. Three-dimensional trajectories were evaluated with a digitized version of the Schaltenbrand–Wahren atlas (AtlasSpace, Elekta).

In an attempt to minimize cerebrospinal fluid leakage and, consequently, intraoperative brain shift, the head of each patient was elevated to approximately 30° from the horizontal plane and a burr hole was made 30–35 mm anterior to the coronal suture and 20–25 mm lateral to the midline. With such a burr hole placement, the electrode was oriented at angles of 40–50° to the horizontal plane of the AC-PC line and 5–10° to the sagittal plane in STN-DBS. This trajectory of the electrode was approximately parallel to the long axis of the STN and ran sequentially through the zona incerta and STN.

A tungsten semimicroelectrode (about 200–400 kohm), guided by an outer cannula (catheter insertion needle for a Leksell stereotactic system) was used for extracellular recording, and the location of the STN was identified electrophysiologically. A DBS lead (model 3387; Medtronic Inc., Minneapolis, MN, USA) with four contact points, numbered 0–3 sequentially from the most distal contact 0 to the most proximal contact 3, was placed in such a way that Contact 0 was located in the ventral portion of the STN and Contact 3 was located at Forel H2 or the zona incerta. Immediately after completion of the stereotactic operation, we performed MR imaging again with the stereotactic frame fixed to the skull, and the location of the electrode was confirmed. The placement of the DBS lead for both sides was carried out by single-stage surgery in all patients (4,18,19). After test stimulation for several days, each DBS lead was implanted and connected to implantable pulse generators (model 7426; Medtronic).

Stimulation Procedures

In our protocol for STN-DBS, stimulation was started by selecting Contact 0 or 1 as the cathode and Contact 3 as the anode, aiming to stimulate a wide area of the STN and supra-STN area. If such bipolar stimulation was insufficient for alleviating neurologic symptoms, monopolar stimulation was then performed. At the time of PET examination, all patients had beneficial effects of their bipolar stimulation. The selected stimulation conditions at PET examination were such that Contact 0 or 1 was taken as the cathode and Contact 3 as the anode, with an intensity and frequency within the ranges of 1.6–2.7 V and 120–150 Hz, respectively; and the pulse width was 150 ms in all patients. On the basis of the stereotactic coordinates of the DBS leads, identified by postoperative MR imaging, the contacts used as the cathode were found to be located in the center or bottom of the STN, and the contacts used as the anode were located at Forel H2 or the zona incerta, just above the STN.

Positron Emission Tomography

To evaluate the effects of STN stimulation, a PET study was performed at approximately one month after surgery. FDG-PET was performed twice on two consecutive days. Before the day of the PET study, DBS was turned off, overnight, for at least 12 hours to create an identical situation for comparison of the effects of STN-DBS between on- and off-stimulation.

On the day of the PET study, DBS was turned on in the morning and left on during the daytime. PET was carried out in the afternoon during the off-period in each case and stimulation was turned off at night. On the next morning, stimulation was kept off during daytime, and PET was carried out in the afternoon during the off-period in each case. The patients were requested to maintain the dose and schedule of their medication stable during the study. They were evaluated using the unified Parkinson's disease rating scale (UPDRS) and Hoehn and Yahr disability scale immediately before and after the PET on each day, and the scores before and after the PET were averaged.

All patients fasted overnight prior to undergoing FDG-PET. During the PET study, each patient was positioned supine in the scanner with a three-dimensional laser alignment of the orbitomeatal line. All PET studies were performed in the three-dimensional mode using PosiCam-HZL (Positron Co., Houston, TX, USA). Two-dimensional image planes with 61 slices were used with an axial field of view of 16.6 cm and a transaxial resolution of 6.1 mm (full width half maximum) in all directions. All subjects underwent the PET study after injection of 350 MBq FDG, and each PET session (on- and off-stimulation) was performed at rest with the eyes closed and with a low ambient auditory noise.

Data Analysis

Differences between the motor score and subscores on the UPDRS during on-stimulation and off-stimulation (DBS off—DBS on) were used for analysis. A difference was considered significant if the p-value was 0.001 or less. Differences in regional FDG uptake level between on- and off-stimulation were analyzed by the paired t-test employing SPM99 software (Wellcome Department of Cognitive Neurology, London, UK), implemented in MATLAB (Mathworks, Sherborn, MA, USA). The scans from each subject were realigned and stereotactically normalized into the atlas of Talairach and Tournoux (20). Subsequently, the images were scaled proportionally and smoothed with an isotopic Gaussian kernel (full width half maximum 12 mm for all directions) to reduce for interindividual anatomical variability and to improve the signal-to-noise ratio. Changes in clusters were accepted as significant if the p-values corrected for multiple comparisons were 0.005 or less. Spearman's rank correlation was used to analyze the relationships between changes in subscores on the UPDRS and changes in rCMRGlc in each cluster. A correlation was considered significant if the p-value was 0.05 or less.

Results

Neurological Improvement Following STN-DBS

In comparison to off-stimulation, a marked neurologic improvement was observed during on-stimulation (Table 1). The UPDRS motor score during the off-period decreased from

TABLE 1. Patient Characteristics

Patient no./sex/age	Age at onset (year)	Dominantly affected side	Handedness	UPDRS part III				Hoehn and Yahr		Medication (mg/day)			
				On-period		Off-period		Off-period		LED		MAO-B inhibitor	
				DBS-off	DBS-on	DBS-off	DBS-on	DBS-off	DBS-on	Pre op	Post op	Pre op	Post op
1/M/42	36	Left	Right	18	11	50	20	5	2.5	1300	650	10	5
2/M/63	53	Left	Right	42	11	49	11	4	1	710	500	0	0
3/F/71	55	Left	Right	21	21	34	24	4	2	300	200	0	0
4/M/76	43	Left	Right	28	24	35	31	4	2.5	445	445	2.5	2.5
5/F/50	48	Right	Right	11	2	26	6	3	0	330	330	0	0
6/M/68	58	Left	Right	13	1	36	6	4	1	1100	1100	5.0	5.0
7/F/63	58	Right	Right	16	0	23	0	3	1	713	713	0	0
8/F/62	49	Left	Right	13	14	51	10	4	2	770	770	0	0
Mean	50			20	11	38.0	14	3.9	1.50	708	588	2.2	1.6
SD	7.67			10	9.1	11	11	0.6	0.9	356	283	3.6	2.3
p-value				0.032*		0.001‡		< 0.001‡		0.179		0.351	

*$p < 0.05$, Wilcoxon single-rank test.
†$p < 0.01$, Wilcoxon single-rank test.
‡$p < 0.001$, Wilcoxon single-rank test.
UPDRS part III, motor ratings on the unified Parkinson's disease rating scale; on- and off-periods, periods of best and worst motor activity in the daytime; LED, levodopa-equivalent dose; MAO-B, monoamine oxidase B; Pre op, before deep brain stimulation of the subthalamic nucleus (STN-DBS); Post op, at the time of [18F]fluorodeoxyglucose-positron emission tomography (FDG-PET) examination.

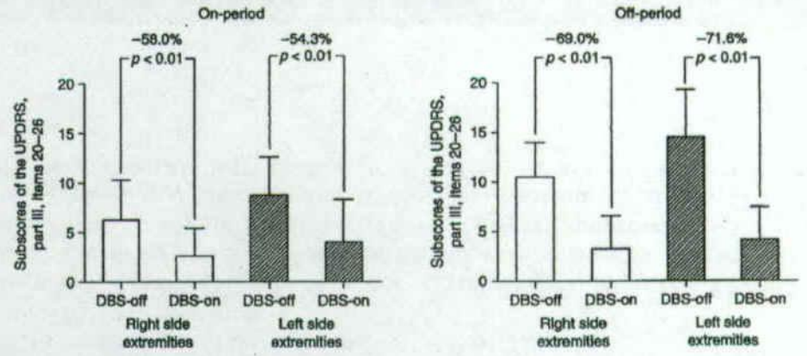

FIGURE 2. Effects of bilateral STN-DBS on the UPDRS motor score (subscores of the UPDRS, part III, items 20–26) as compared between the right and left extremities. Statistical significance was determined by Wilcoxon single-rank test. STN-DBS, deep brain stimulation of the subthalamic nucleus; UPDRS, unified Parkinson's disease rating scale.

38.0 ± 10.9 to 13.5 ± 10.5 ($p < 0.001$), and the mean Hoehn and Yahr disability scale during the off-period decreased from 3.88 ± 0.64 to 1.50 ± 0.89 ($p < 0.001$).

All eight patients were right hand dominant cases. The UPDRS motor score of the left side extremities (subscores of the UPDRS, part III, items 20–26), during the off-period, decreased from 14.50 ± 4.81 to 3.88 ± 3.04 ($p < 0.01$) following bilateral STN-DBS. The UPDRS motor score of the right side extremities (subscores of the UPDRS, part III, items 20–26), during off-period, also decreased from 10.50 ± 3.55 to 3.25 ± 3.33 following bilateral STN-DBS ($p < 0.01$) (Fig. 2). When comparing medication use after surgery to medication use before surgery, the LED during the PET study decreased from 708.4 ± 355.9 to 588.4 ± 282.8 mg/day, and the dose of MAO-B inhibitor decreased from 2.19 ± 3.64 to 1.56 ± 2.29 mg/day (Table 1). Because three out of eight patients in the present study did not take sufficient doses of levodopa, even before surgery, due to unbearable side-effects, no significant decreases were noted during the PET study in terms of either the LED or dose of MAO-B inhibitor.

Changes in rCMRGlc Induced by STN-DBS

Compared to the situation with that during off-stimulation, extended clusters of increased rCMRGlc were observed during on-stimulation in the right middle frontal gyrus corresponding to the premotor area (BA 6; $x = 24$, $y = 2$, $z = 58$; and $x = 16$, $y = -6$, $z = 58$), and in the right anterior lobe of the cerebellum ($x = 14$, $y = -44$, $z = -14$; Table 2). No similar changes in rCMRGlc were found in either the left middle frontal gyrus or the left anterior lobe of the cerebellum. There were no clusters of significantly decreased rCMRGlc seen (Fig. 3).

Relationship of Motor Symptoms to rCMRGlc

Among the items of the UPDRS motor score, resting tremor of the left extremity ($r^2 = 0.828$, $p < 0.02$) and rigidity of the left extremity ($r^2 = 0.368$, $p < 0.05$) showed clear correlations with changes seen in rCMRGlc in the right

TABLE 2. Brain Regions With a Significantly Altered rCMRGlc on FDG-PET During Bilateral STN-DBS, Ordered According to Their Peak Z-scores

Region	Talairach coordinates			Z_{max}	Voxels per cluster
	x	y	z		
Increased rCMRGlc					
Right middle frontal gyrus	24	2	58	4.02	185
	16	−6	58	3.7	
Right rostral cerebellar lobe	14	−44	−14	3.53	103

Peak activations ($p < 0.001$, > 32 voxels) in the left-right (x), anterior-posterior (y), and superior-inferior (z) planes (20). rCMRGlc, regional cerebral metabolic rate of glucose.

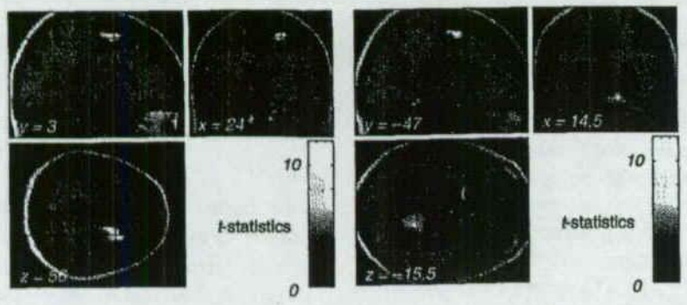

FIGURE 3. Regions associated with significant changes in rCMRGlc (DBS on—DBS off) as measured with SPM99 ($p < 0.005$ for cluster level corrected for multiple comparisons; color bars represent *t*-values). The figure shows transverse, sagittal, and coronal views in projection onto brain slices of a standard MRI (*x*/*y*/*z* coordinates according to the atlas of Talairach and Tournoux). rCMRGlc, Regional cerebral metabolic rate of glucose; MRI, magnetic resonance imaging; PD, Parkinson's disease; DBS, deep brain stimulation.

premotor area, but not with that in the right anterior cerebellum. Other items of the UPDRS motor score, such as speech, facial expression, resting tremor of the head and neck, action or postural tremor of the hands, rigidity of the neck, motor performance of the hands and legs, arising from a chair, posture, gait, postural stability, and body bradykinesia and hypokinesia, revealed no significant correlations with changes seen in rCMRGlc, in either the right premotor area or the right anterior cerebellum (Table 3).

Discussion

Changes in Cerebral Activity Induced by STN-DBS

In this study, changes in rCMRGlc were detected

TABLE 3. Correlations Between Unified Parkinson's Disease Rating Scale (UPDRS) Subscores and Changes of Regional Cerebral Metabolic Rate of Glucose (rCMRGlc) in the Right Premotor Area and Right Rostral Cerebellum

			p-values	
UPDRS part III subcategories		Changes of UPDRS scores (DBS_{on}–DBS_{off})	Right premotor area	Right rostral cerebellum
18. Speech		−1.309 ± 0.463	0.7686	0.4925
19. Facial expression		−1.356 ± 0.479	0.8455	0.3805
20. Tremor at rest	face and neck	−0.250 ± 0.463	0.0956	0.505
	left	−1.125 ± 0.398	0.0156*	0.3775
	right	−1.250 ± 0.366	–	0.0722
21. Action or postural tremor of hands	left	−0.750 ± 0.707	0.4687	0.945
	right	−0.625 ± 0.744	–	0.0728
22. Rigidity	neck	−1.125 ± 0.835	0.2301	0.9203
	left	−2.625 ± 1.188	0.0462*	0.819
	right	−1.625 ± 1.302	–	0.601
23+24+25+26 (finger taps, hand movements, alternating movements of hands, and leg agility)	left	−4.750 ± 3.495	0.1859	0.1658
	right	−3.750 ± 2.816	–	0.7528
27. Arising from a chair		−0.875 ± 1.126	0.6123	0.8925
28. Posture		−1.000 ± 1.069	0.2083	0.0851
29. Gait		−1.250 ± 1.165	0.5403	0.5403
30. Postural stability		−1.500 ± 1.309	0.3775	0.7438
31. Body bradykinesia and hypokinesia		−1.625 ± 0.916	0.1876	0.5209
Total score on UPDRS part III		−25.250 ± 14.130	0.1939	0.447

*$p < 0.05$, Spearman's rank correlation test. DBS, deep brain stimulation.

in the premotor area (BA6) and the anterior lobe of the cerebellum. Previous PET studies (9–15) have demonstrated various areas, such as the supplementary motor area, premotor area, dorsolateral prefrontal cortex, and anterior cingulate gyrus (11,13,14,21), activated or deactivated by STN-DBS.

One obvious cause of variability in the results of PET studies is differences in study design. Changes in cerebral activity may be dependent on the nature of the tasks employed during these PET studies. In the present study, FDG-PET was performed at rest without the execution of motor tasks. The observed changes in rCMRGlc can thus be related to motor symptoms at rest. For example, changes related to postural tremor may not be detected using such a study design. Consistent with our findings, Limousin et al. (11) reported that when the effect of STN-DBS at rest is examined, reqional cerebral blood flow undergoes increases in the sensorimotor (BA 4) and premotor (BA 6) areas.

Another possible cause of the variability in results of PET studies may be differences in location of the DBS leads. In previous PET investigations, the location of the DBS leads has not always been specified in detail. We implanted DBS leads with a sagittal plane angle of approximately 45° with reference to the AC–PC line. All of our patients preferred stimulation of the STN together with areas just above the STN (4).

Clinical observations have shown that stimulation of areas just above the STN can produce a marked attenuation of tremor, rigidity, and levodopa-induced dyskinesia. Anatomical studies have demonstrated that many pathways that are involved in motor control, such as cerebellothalamic, pallidothalamic, and pallidosubthalamic fibers, pass through these areas. Future PET studies need to analyze the relationship between the locations of the DBS leads and activated or deactivated areas.

Correlation of Motor Symptoms With Activity of the Premotor Area

Previous PET studies have not included detailed examinations of the relationships between improvements of the symptoms and activated or deactivated areas. The present findings indicated that the rCMRGlc of the right prefrontal area increased in association with attenuation of resting tremor and rigidity of the left extremities.

Although the STN was stimulated bilaterally, a strong lateralization of the stimulation-induced changes was observed on the right side. The most probable explanation for such lateralization was the predominance of symptoms on the left side in the patients included in this study: six out of eight patients demonstrated predominant symptoms on the left side (Table 1). This could have led to a greater chance of detecting changes in rCMRGlc on the right side and their correlation to an improvement of symptoms on the left side. Such an inference implies that changes in activity of the premotor area are closely related to tremor at rest on the contralateral side.

Mechanisms of Changes in rCMRGlc

The efferents of the STN mediate information to the premotor area via pallidothalamic and thalamocortical fibers, whereas the cerebellar afferents project predominantly to the primary motor area via thalamocortical fibers (19,22–24). It is possible that STN-DBS may activate the premotor area through pallidothalamic and thalamocortical fibers. Another possibility is that changes in the activity of the premotor area are the result, rather than the cause, of attenuation of resting tremor and rigidity. According to recent human imaging studies, the premotor area plays an important role in spatial attention and memory (25,26), or the planning and execution of voluntary movements (27–29). Simon et al. (24) demonstrated, in a functional MR imaging study, that motor preparation is mainly related to the caudal portion of the premotor area, whereas the more rostral portion is involved in spatial attention and memory. It appears possible, therefore, that the activity of the premotor area is deactivated in patients with resting tremor and rigidity, which would presumably disturb the appropriate processing of motor

preparation, and such deactivation becomes normalized when these symptoms are controlled by STN-DBS. If this inference is in fact correct, the observed increase in rCMRGlc in the present study could represent a normalization of the deactivation, rather than a direct activation, of the premotor area.

The effects of STN-DBS on changes in activity of the cerebellum remain controversial. Hilker et al. (30) reported that the rCMRGlc in the anterior cerebellum is decreased by STN-DBS. In contrast, Vafaee et al. (15) observed an increase in regional cerebral metabolic rate of oxygen consumption in the cerebellum during STN-DBS. The activation of the anterior lobe of the cerebellum detected in this study could be accounted for by antidromic activation of the cerebellothalamic fibers passing through the areas just above the STN (31) (vida supra). The detailed relationships between the location of the DBS leads and activation of the anterior lobe of the cerebellum need to be determined in future studies.

Conclusions

The present data suggest that STN-DBS normalizes deactivation of the premotor area in association with control of resting tremor and rigidity of the contralateral extremities. Such an inference, in turn, implies that resting tremor and rigidity may disturb appropriate processing of motor preparation within the premotor area in patients with PD. These FDG-PET findings are consistent with the idea that STN-DBS modifies the activities of neural circuits involved in motor control.

Acknowledgments

This work was supported by Grants-in-Aid for Scientific Research from the Ministry of Education, Culture, Sports, Science and Technology, Japan (nos. A12307029 and A15209047), by grants from the Ministry of Education, Culture, Sports, Science and Technology for the promotion of industry–university collaboration at Nihon University, and a program grant from the Ministry of Health, Labor and Welfare, Japan.

References

1. Benabid AL, Pollak P, Gross C et al. Acute and long-term effect of subthalamic nucleus stimulation in Parkinson's disease. *Stereotact Funct Neurosurg* 1994;62:76–84.

2. Brown RG, Dowsey PL, Brown P et al. Impact of deep brain stimulation on upper limb akinesia in Parkinson's disease. *Ann Neurol* 1999;45:473–488.

3. Burchiel KJ, Anderson VC, Favre J et al. Comparison of pallidal and subthalamic nucleus deep brain stimulation for advanced Parkinson's disease: results of a randomized, blind pilot study. *Neurosurgery* 1999;45:1375–1382.

4. Katayama Y, Kasai M, Oshima H et al. Subthalamic nucleus stimulation for Parkinson disease: benefits observed in levodopa-intolerant patients. *J Neurosurg* 2001;95:213–221.

5. Krack P, Batir A, Van Blercom N et al. Five-year follow-up of bilateral stimulation of the subthalamic nucleus in advanced Parkinson's disease. *N Eng J Med* 2003;349:1925–1934.

6. Kumar R, Lozano AM, Sime E et al. Comparative effects of unilateral and bilateral subthalamic nucleus deep brain stimulation. *Neurology* 1999;53: 561–566.

7. Limousin P, Krack P, Pollak P et al. Electrical stimulation of the subthalamic nucleus in advanced Parkinson's disease. *N Eng J Med* 1998;339:1105–1111.

8. Moro E, Scerrati M, Romito LMA et al. Chronic subthalamic nucleus stimulation reduces medication requirements in Parkinson's disease. *Neurology* 1999;53:85–90.

9. Antonini A, Landi A, Benti R et al. Functional neuroimaging (PET and SPECT) in the selection and assessment of patients with Parkinson's disease undergoing deep brain stimulation. *J Neurosurg Sci* 2003;47:40–46.

10. Brooks DJ, Samuel M. The effects of surgical treatment of Parkinson's disease on brain function: PET findings. *Neurology* 2000;55 (12 Suppl. 6):S52–S59.

11. Limousin P, Krack P, Pollak P et al. Changes in cerebral activity pattern due to subthalamic nucleus or internal pallidum stimulation in Parkinson's disease. *Ann Neurol* 1997;43:283–291.

12. Sestini S, Scotto di Luzio A, Ammannati F et al. Changes in regional cerebral blood flow caused by deep-brain stimulation on the subthalamic nucleus in Parkinson's disease. *J Nucl Med* 2002;43:725–732.

13. Strafella AP, Sadikot AF, Dagher A. Subthalamic deep brain stimulation does not induce striatal dopamine release in Parkinson's disease. *NeuroReport* 2003;14:1287–1289.

14. Thobois S, Dominey P, Fraix V et al. Effects of subthalamic nucleus stimulation on actual and imagined movement in Parkinson's disease: a PET study. *J Neurol* 2002;249:1689–1698.

15. Vafaee MS, Ostergaard K, Sunde N et al. Focal changes of oxygen consumption in cerebral cortex of patients with Parkinson's disease during subthalamic stimulation. *NeuroImage* 2004;22:966–974.

16. Raichle ME, Gusnard DA. Appraising the brain's energy budget. *Proc Natl Acad Sci USA* 2002;99:10237–10239.

17. The Deep-brain Stimulation for Parkinson's Disease Study Group. Deep-brain stimulation of the subthalamic nucleus or the pars interna of the globus pallidus in Parkinson's disease. *N Engl J Med* 2001;345:956–963.

18. Yamamoto T, Katayama Y, Fukaya C et al. New method of deep brain stimulation therapy with two electrodes implanted in parallel and side by side. *J Neurosurg* 2001;95:1075–1078.

19. Yamamoto T, Katayama Y, Kano T et al. Deep brain stimulation for the treatment of parkinsonian, essential, and post-stroke tremor: suitable stimulation method and changes of effective stimulation intensity. *J Neurosurg* 2004;101:201–209.

20. Talairach J, Tournoux P. *Co-planar stereotactic atlas of the human brain: 3-dimension proportional system: an approach to cerebral imaging*. Stuttgart, Germany: George Thieme Verlag, 1988.

21. Ceballos-Baumann AO, Boecker H, Bartenstein P et al. A positron emission tomographic study of subthalamic nucleus stimulation in Parkinson's disease: enhanced movement-related activity of motor association cortex and decreased motor cortex resting activity. *Arch Neurol* 1992;56:997–1003.

22. Lehericy S, Grand S, Pollak P et al. Clinical characteristics and topography of lesions in movement disorders due to thalamic lesions. *Neurology* 2001;57:1055–1066.

23. Star PA, Vitek JL, Bakay RAE. Deep brain stimulation for movement disorders. *Neurosurg Clin N Am* 1998;9:381–402.

24. Simon SR, Meunier M, Piettre L et al. Spatial attention and memory versus motor preparation: premotor cortex involvement as revealed by fMRI. *J Neurophysiol* 2002;88:2047–2057.

25. Courtney SM, Petit L, Maisog JM et al. An area specialized for spatial working memory in human frontal cortex. *Science* 1998;279:1347–1351.

26. Stern CE, Owen AM, Tracey I et al. Activity in ventrolateral and mid-dorsolateral prefrontal cortex during nonspatial visual working memory processing: evidence from functional magnetic resonance imaging. *NeuroImage* 2000;11:392–399.

27. Deiber MP, Ibanez V, Sadato N et al. Cerebral structures participating in motor preparation in humans: a positron emission tomography study. *J Neurophysiol* 1996;75:233–247.

28. Grafton ST, Fagg AH, Arbib MA et al. Dorsal premotor cortex and conditional movement selection: a PET functional mapping study. *J Neurophysiol* 1998;79:1092–1097.

29. Van Oostende S, Van Hecke P, Sunaert S et al. FMRI studies of the supplementary motor area and the premotor cortex. *NeuroImage* 1997;6:181–190.

30. Hilker R, Voges J, Weisenbach S et al. Subthalamic nucleus stimulation restores glucose metabolism in associative and limbic cortices and in cerebellum: evidence from a FDG-PET study in advanced parkinson's disease. *J Cereb Blood Flow Metab* 2004;24:7–16.

31. Naus CG, Flumerfelt BA, Hrycyshyn AW. Topographic specificity of aberrant cerebellorubral projections following neonatal hemicerebellectomy in the rat. *Brain Res* 1984;20:1–15.

Neuromodulation

Technology at the Neural Interface

VOLUME XI • NUMBER 4 • NOVEMBER 2008

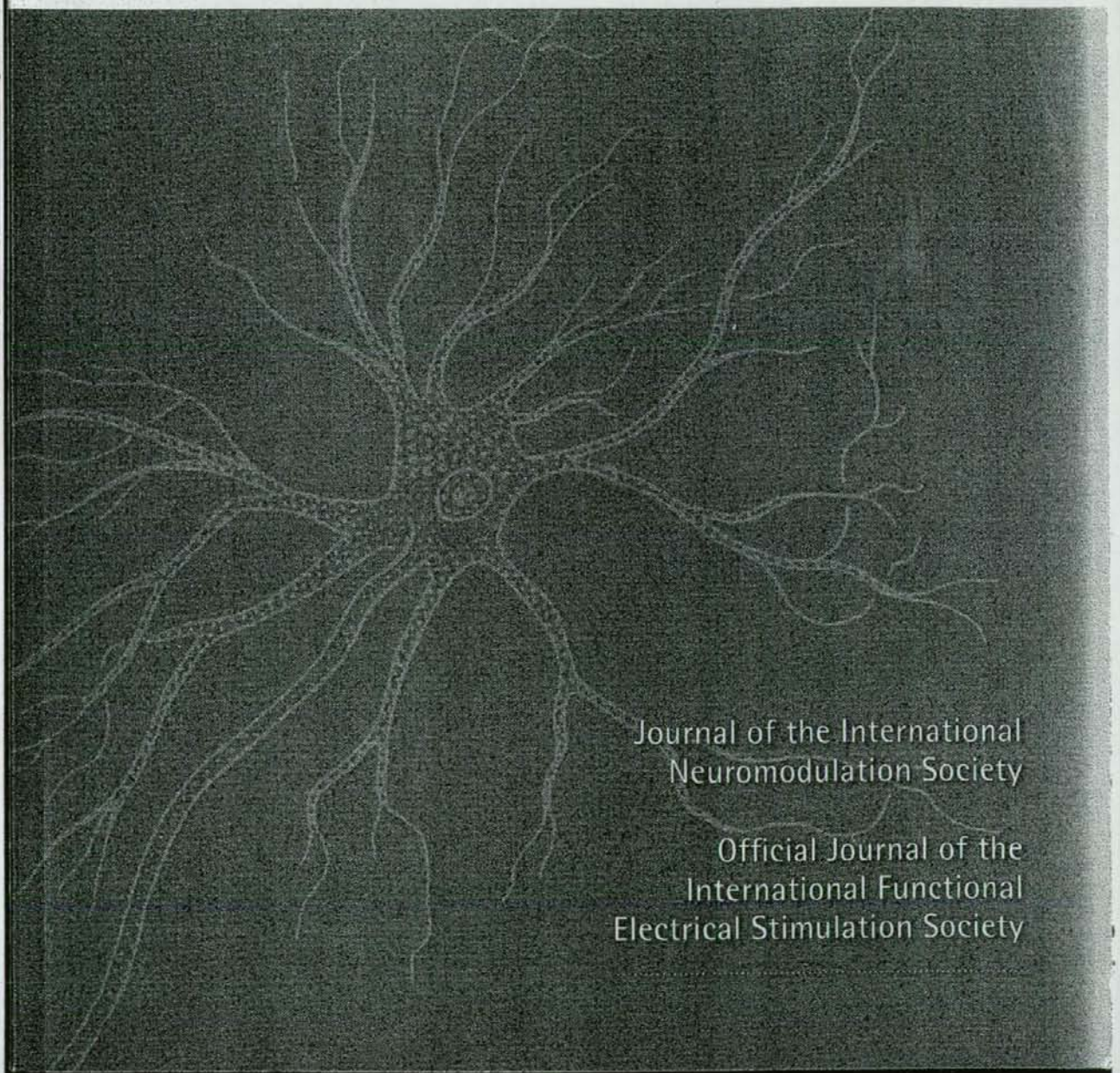

Journal of the International Neuromodulation Society

Official Journal of the International Functional Electrical Stimulation Society

Volume 11 • Number 4 • 2008
http://www.blackwell-synergy.com/loi/ner

ORIGINAL ARTICLE

Direction and Predictive Factors for the Shift of Brain Structure During Deep Brain Stimulation Electrode Implantation for Advanced Parkinson's Disease

Toshiki Obuchi, MD* • Yoichi Katayama, MD, PhD*† • Kazutaka Kobayashi, MD, PhD*† • Hideki Oshima, MD, PhD* • Chikashi Fukaya, MD, PhD*† • Takamitsu Yamamoto, MD, PhD*†

Department of Neurological Surgery and Division of Applied System Neuroscience, †Department of Advanced Medical Science, Nihon University School of Medicine, Tokyo, Japan

ABSTRACT

Objectives. The aims of this study were to clarify the direction and degree of brain shift, and to determine the predictive factors for a brain shift during deep brain stimulation (DBS) of the subthalamic nucleus (STN). **Materials and Methods.** To evaluate the brain shift during bilateral STN-DBS, the position of the anterior commissure (AC), posterior commissure (PC), midcommissure point (MC), and tip of the frontal lobe and anterior horn of the lateral ventricle were calculated pre- and poststereotactic operations in the three-dimensional direction employing special software (Leksell SurgiPlan). To determine the predictive factors for a brain shift, patient's age, operation hours, width of the third ventricle, bicaudate index (BCI), and cella media index (CMI) were compared with the shift of MC. **Results.** In 50 patients, the MC shifted mainly in the posterior direction (*y*-axis: 1.27 ± 0.7 mm), and the shifts in the inferior direction (*z*-axis: 0.11 ± 0.43 mm) and lateral direction (*x*-axis: 0.02 ± 0.39 mm) were small. The shift of the MC in the posterior direction correlated well with the shift of the tip of the anterior lobe and anterior horn. Among the predictive factors examined, namely, the patient's age, operation hours, width of the third ventricle, BCI, and CMI, only the CMI showed a correlation with the shift of the MC ($r = 0.42$, $p < 0.01$, Pearson's correlation coefficient; and $p < 0.05$, logistic regression analysis). **Conclusions.** In bilateral STN-DBS, brain shift occurred mainly in the posterior direction, and the CMI is useful for the prediction of a brain shift. Enlargement of the body part of the lateral ventricle is the most reliable factor for predicting a brain shift.

KEY WORDS: *Brain shift, deep brain stimulation, Parkinson's disease, stereotactic operation, STN-DBS.*

Introduction

The recent marked increase in a number of patients who undergo deep brain stimulation (DBS), especially subthalamic nucleus (STN)-DBS, reflects the efficacy of this therapy (1–5), and accuracy of electrode placement is required for success of this therapy (6–9). Brain shift occurs after the skull and dura have been opened during the stereotactic operation, and this brain shift decreases the accuracy of target coordination calculated on the basis of preoperative magnetic resonance imaging (MRI) carried out when the skull is closed. An intraoperative brain shift is caused mainly by the outflow of cerebrospinal fluid (CSF) and by the influx of air into the intracranial space. Such intracranial air influx is caused not only by the CSF outflow, but also by a decreased intracranial blood volume.

Therefore, we fixed the angle of head elevation and the location of the burr hole during the STN-DBS procedure, and examined the MR images obtained before and immediately after implantation of the DBS electrode to compare the shift of brain structures occurring during the stereotactic operation.

In the present study, we attempted to clarify the direction and degree of brain shift during the stereotactic operation. In addition, we also attempted to determine the predictive factors for a brain shift that were recognizable before the stereotactic operation.

Submitted: October 23, 2007; accepted: February 20, 2008. Address correspondence and reprint requests to: Takamitsu Yamamoto, MD, PhD, Division of Applied System Neuroscience, Department of Advanced Medical Science, Nihon University School of Medicine, 30-1 Ohyaguchi Kamimachi, Itabashi-ku, Tokyo 173-8610, JAPAN. Email: nusmyama@med.nihon-u.ac.jp

Materials and Methods

Patient Population

Fifty patients (100 sides) with advanced Parkinson's disease treated by bilateral STN-DBS participated in this study. DBS was performed with the informed consent of each patient and family. The 50 patients consisted of 23 men and 27 women. The age range was from 44 to 76 years old, and the mean age was 63.5 ± 6.6 years old.

Surgical Procedures

After the patient had received a local anesthetic, a Leksell Series G head frame (Elekta Instrument AB, Stockholm, Sweden) was fixed to the skull. With the MRI indicator attached to the stereotactic head frame, MR imaging was carried out at a 1-mm slice thickness, and the anterior commissure (AC) and posterior commissure (PC) were identified with special software (Leksell SurgiPlan, Elekta Instrument AB) (Fig. 1). Fixing the head elevation at between 25 and 30 degrees from the horizontal plane of the ground surface and under local anesthesia, a dual-floor burr hole (15 mm in diameter) (10) was created 30 to 35 mm anterior to the coronal suture and 20 to 25 mm lateral to the midline.

The right side was always operated on first, but the burr hole was made bilaterally at first during the planning of the first trajectory. The dura was kept intact, and the burr hole was stuffed with a cotton sheet soaked in saline. After removing the right-side cotton sheet, the dura of the right burr hole was opened and the arachnoid membrane and cortical surface also were coagulated at the point of electrode insertion. The dura of the left-side burr hole was opened after a permanent DBS electrode (model 387; Medtronic Inc., Minneapolis, MN, USA) was implanted and fixed to the skull with the burr-hole ring and burr-hole cap included in the package of the DBS electrode.

The target was then approached from the burr hole at an angle of from 40 to 50 degrees to the horizontal plane of the AC–PC line (Fig. 2). Three-dimensional trajectory visualization and a digitized version of the Schaltenbrand–Wahren atlas (AtlasSpace, Elekta Instrument AB) were employed to confirm the structure through which the electrode passed (11). A microelectrode guided by an outer cannula was inserted into the STN region through a frontal burr hole to confirm the location of the STN, and a permanent DBS electrode for STN-DBS was implanted. A one-time bilateral operation was the choice of all patients. After finishing the bilateral electrode implantation, the first operation was completed. An implantable pulse generator was implanted under the anterior chest wall, and connected to the DBS electrode on a separate day under general anesthesia.

Calculation of the Shift of Brain Structures

Immediately after completion of the stereotactic operation and without implantable pulse generator implantation, we examined the MR images obtained again, while the sterotactic frame was still fixed to the skull and the MRI indicator was attached to the head frame. The location of the DBS electrode was confirmed on the SurgiPlan, and the difference between the pre- and postoperative coordinates of the AC, PC, midcommissure (MC), and tip of the frontal lobe and anterior horn was calculated as the index of brain shift. We also calculated the width of the third ventricle, bicaudate index (BCI; distance between the caudate nuclei divided by the maximum width between the frontal horns of the lateral ventricles), and cella media index (CMI; minimum width between the lateral ventricles at the cella media level divided by the cranial width at the same level) using the SurgiPlan before the operation (Fig. 3). To determine the predictive factors for a brain shift, we examined the correlation of patient's age, operation hours, width of the third ventricle, BCI, and CMI with the shift of the MC in the three-dimensional direction.

Statistical Analysis

Statistical analyses were performed using Pearson's correlation coefficient and logistic regression analysis. In this article, values for groups are expressed as the means ± standard deviation.

Results

Shift of the Frontal Lobe, Anterior Horn, and MC

The right side was always operated on first, and the location of the STN was investigated and identified by microelectrode recording. Once the right-side location of the STN had been identified by the microelectrode recording, the left-side identification of the STN by microelectrode

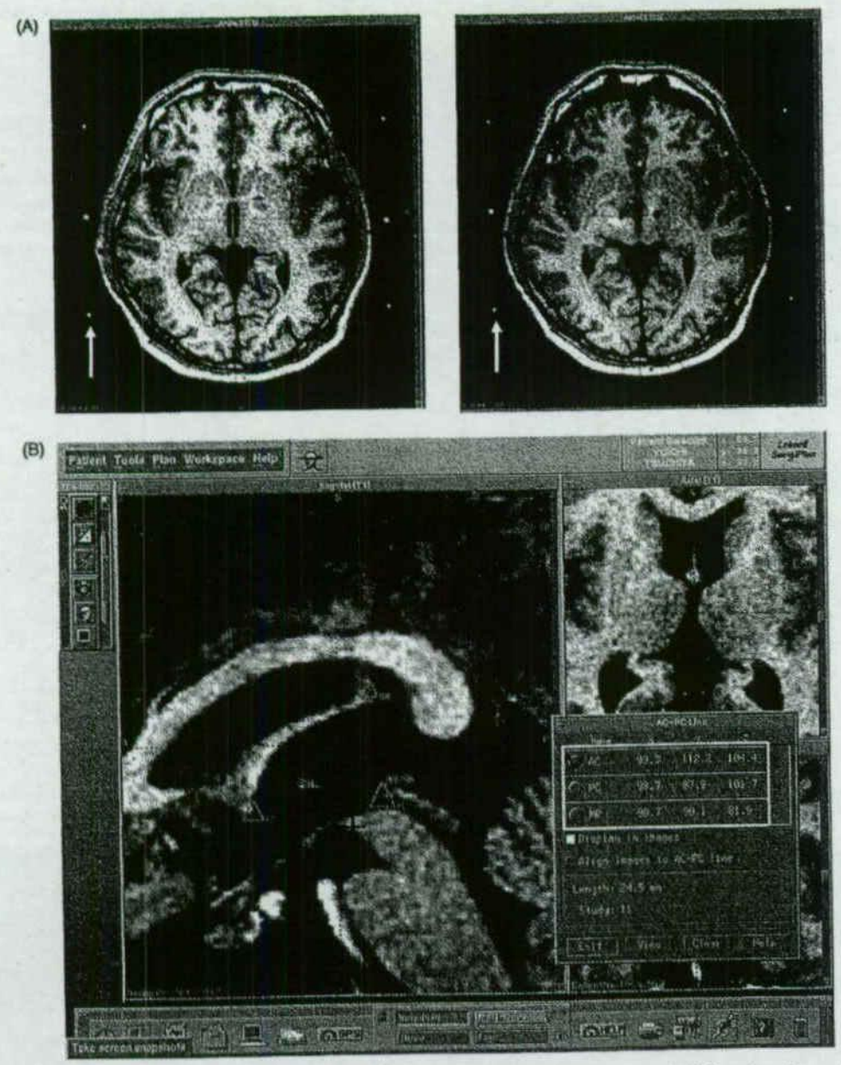

FIGURE 1. Comparison of the shift of midline structures employing SurgiPlan. (A) MRI indicator, which has six point markers (arrow), is fixed to the stereotactic head frame, and MRI data were transferred to SurgiPlan. The three-dimensional coordinates of the anterior commissure (AC), posterior commissure (PC), and midcommissure (MC) were compared between pre- and poststereotactic operations. On a postoperative MR imaging (right), an artifact of the deep brain stimulation electrode implanted into the subthalamic nucleus region can be observed. Green triangles indicate the points of AC and PC. (B) AC and PC (Green triangles) are identified on the sagittal plane of SurgiPlan. Three-dimensional coordinates of AC and PC were calculated using SurgiPlan (yellow rectangular area).

recording was easy and yielded almost the same three-dimensional coordinates as for the right side. The cortical surface sank during the microelectrode mapping and DBS electrode placement. Comparison of the pre- and postoperative MR images obtained in the spinal position revealed that the tip of the frontal lobe shifted mainly in the posterior direction (5.47 ± 2.22 mm on the right side and 5.13 ± 2.19 mm on the left side). The tip of the

TABLE 1. Brain Shift of Each Landmark Calculated Between Pre- and Poststereotactic Operations

	Shift (mm)					
	X (right–left)		*Y* (anterior–posterior)		*Z* (superior–inferior)	
	Mean ± SD	Maximum	Mean ± SD	Maximum	Mean ± SD	Maximum
Tip of right frontal lobe	2.20 ± 3.98	12.00	−5.47 ± 2.22	−10.10	0.63 ± 6.91	−19.80
Tip of left frontal lobe	−1.14 ± 2.99	−10.7	−5.13 ± 2.19	−11.70	0.69 ± 5.81	17.20
Tip of right anterior horn	0.54 ± 1.09	3.70	−3.69 ± 1.88	−8.70	0.63 ± 1.29	3.60
Tip of left anterior horn	−0.65 ± 1.22	−4.80	−3.26 ± 1.94	−8.10	0.63 ± 1.12	3.9
Midcommissure	−0.02 ± 0.39	−1.20	−1.27 ± 070	−3.45	−0.11 ± 0.43	1.00

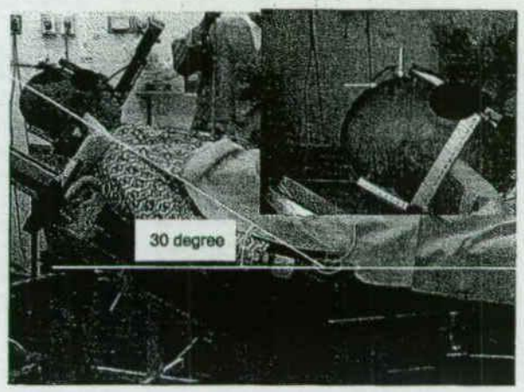

FIGURE 2. Head elevation and location of burr hole during the stereotactic operation. Head elevation is restricted to be under 30 degrees, and the burr hole (vertical arrow) is located 30 to 35 mm anterior to the bregma (horizontal arrow).

anterior horn also shifted mainly in the posterior direction (3.67 ± 1.88 mm on the right side and 3.26 mm on the left side). The MC also shifted mainly in the posterior direction (*y*-axis: 1.27 ± 0.7 mm), and the shifts in the inferior direction (*z*-axis: 0.11 ± 0.43 mm) and lateral direction (*x*-axis: 0.02 ± 0.39 mm) were small (Table 1).

The shift of the MC in each patient was plotted in the axial and sagittal planes (Fig. 4). The shift of the MC in the posterior direction correlated with the shift of the tip of the anterior lobe ($r = -0.59$ on the right side, $r = -0.50$ on the left side; Pearson's correlation coefficient) and with that of the tip of the anterior horn ($r = -0.63$ at the right, $r = -0.68$ at the left; Pearson's correlation coefficient) (Fig. 5).

Predictive Factors for Brain Shift

We examined the correlation of the postoperative shift of the MC in the posterior direction with the width of the third ventricle, BCI, CMI, age, and operation hours. Among these factors, only the CMI revealed a correlation with the shift of the MC ($r = 0.42$, $p < 0.01$; Pearson's correlation coefficient) (Fig. 6). Depending on the extent of the shift of the MC in the posterior direction, the patients were classified into two groups: one showing a shift of more than 1.5 mm ($N = 16$) and the other showing a shift of less than 1.5 mm ($N = 34$). Logistic regression analysis for these two groups suggested that the two groups demonstrated a significant difference in their CMI only ($p = 0.0157$) (Table 2).

Discussion

In the present study, the head elevation was fixed at between 25 and 30 degrees, and the burr hole was made 30 to 35 mm anterior to the bregma. This procedure enabled us to create the burr hole at the highest position on the cranium during the stereotactic operation and to reduce the overflow of CSF from the burr hole (1,11,12). Moreover, the trajectory of the electrode from this burr-hole point allowed passage through the STN over the longest distance. In the condition of cranial opening, when we elevated the head over 30 degrees, the inflow of air into the intracranial space increased with decrease in the volume of intracranial venous blood. We have not employed tissue sealants such as fibrin glue during the operation, and the space of the burr hole around the outer cannula

TABLE 2. Logistic Regression Analysis of the Posterior Shift of Midcommissure for Two Groups Showing Shifts Over 1.5 mm and Under 1.5 mm

	OR	95% CI	*p*-value
Age	0.965	0.86–1.082	0.54
Third ventricle	0.834	0.518–1.344	0.4562
Bicaudate index	0.831	0.587–1.177	0.2968
Cella media index	1.67	1.102–2.532	0.0157
Time	0.994	0.980–1.009	0.4484

95% CI: 95% confidence intervals; OR, odds ratio.

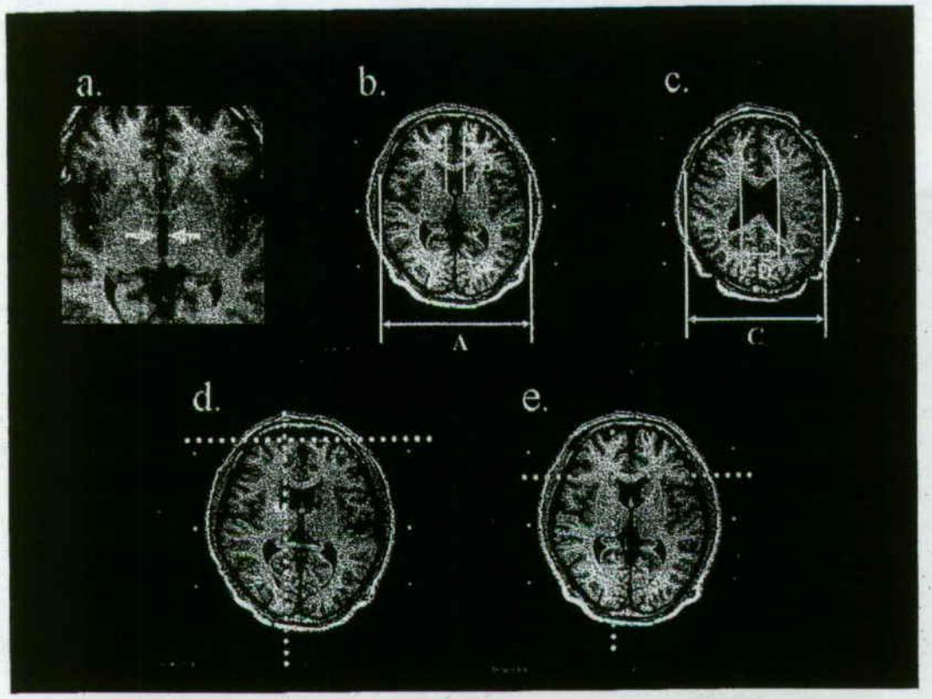

FIGURE 3. Calculation method and calculation points on SurgiPlan. (a) Width of the third ventricle. (b) Bicaudate index (BCI): B/A. (c) Cella media index (CMI): D/C. (d) Tip of the frontal lobe: Three-dimensional coordinates of cross points were compared between pre- and postoperation. (e) Tip of the anterior horn of the lateral ventricle: Three-dimensional coordinates of cross points were compared between pre- and postoperation.

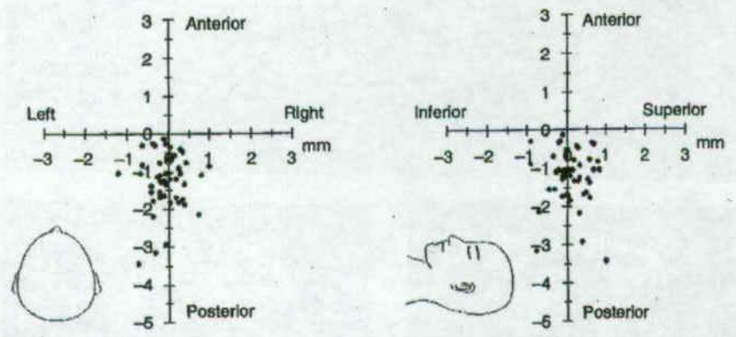

FIGURE 4. Shift of midcommissure (MC). Three-dimensional coordinate of MC (each dot), calculated immediately after the operation, was compared with the coordinate of MC calculated before the operation (cross point of each axis). Left indicates the axial plane, and right indicates the sagittal plane.

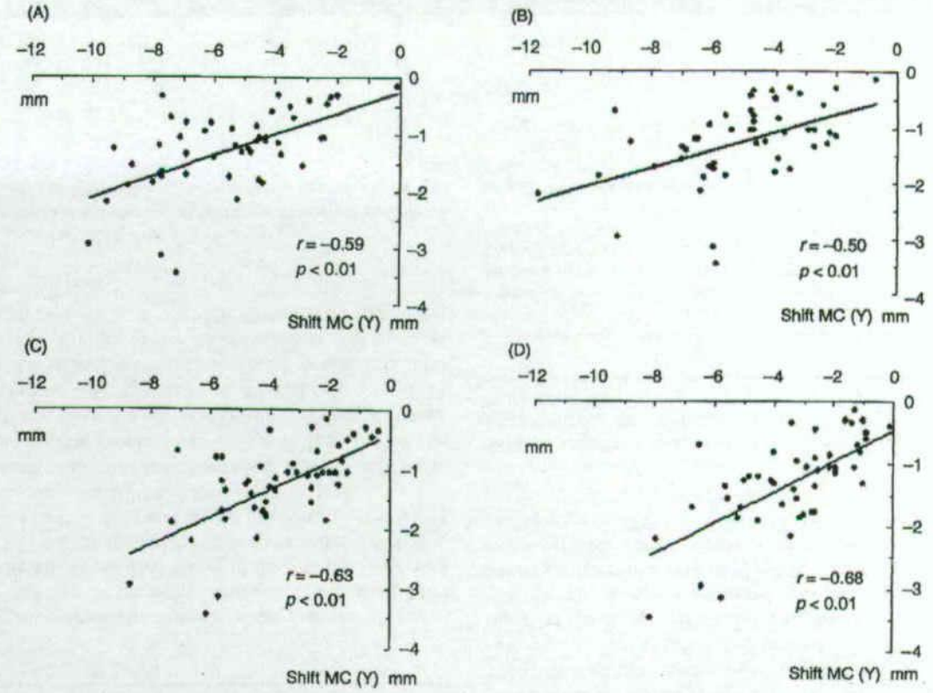

FIGURE 5. Comparison between the posterior shift of midcommissure (MC) and the tip of frontal lobe and anterior horn of the lateral ventricle. (A) Tip of right frontal lobe. (B) Tip of left frontal lobe. (C) Tip of right anterior horn. (D) Tip of left anterior horn.

for the microelectrode recording was stuffed with a cotton sheet soaked in saline. We used SurgiPlan to evaluate the three-dimensional coordinates of the brain structures, and the MC was selected as the indicator of brain shift, because the MC is located in the center of the midline structures and the AC and PC are accurate indicators for the stereotactic coordinates. As compared with the shift of the cortical surface, the shift of the MC was small and the width of the third ventricle demonstrated no significant change in our study.

Wester and Krakenes (13) have described results for stereotactic thalamotomy performed in the sitting position, and concluded that the brain mainly shifted vertically. They calculated the extent to which the cortical surface sank during the stereotactic operation, and concluded that the brain shift at the thalamic level should be estimated at about one-half of the extent of the operative sinking of the cortical surface. Pollo et al. (14) made a 3-mm twist drill hole for STN-DBS, and the dura mater was opened such that the diameter of the opening did not exceed that of their guiding tubes to prevent CSF leakage. They examined the location of the DBS electrode after the stereotactic operation, and the distances between the electrode and the expected and actual targets in the x- and y-axes were found to be 1.34 ± 1.02 mm and 1.03 ± 0.76 mm, respectively. In the z-axis, 39.7% of the stimulation contact points were located proximal to the target, and they concluded that the caudal brain shift depends on the head position and may occur during the implantation procedure. Winkler et al. (15) applied deformity analysis to pre- and postoperative three-dimensional MR images, and found that the brain shift occurred mainly in the posterior direction. The surface of the frontal cortical brain shifted 13 mm, and the region of the subthalamic nucleus revealed a 2-mm shift. In our study, in which the head elevation was restricted to under 30 degrees, the shift of the MC was mainly in the posterior direction, and the shifts in the lateral and inferior directions were small. Subdural air was always detected in the frontal subdural space.

Star et al. (9) reported that 19 (25%) of their 76 STN-DBS procedures showed a change of 2 mm or greater in the lateral or anteroposterior direction, and these changes did not appear to be associated with any particular age group, brain size, or degree of brain atrophy. We examined